

# Sensitivity Monitor Report for the STIS First-Order Modes

---

Nolan R. Walborn and Ralph C. Bohlin  
Space Telescope Science Institute  
October 1998

---

## ABSTRACT

*The sensitivity of the STIS first-order CCD and MAMA modes has been monitored by observations of standard stars for over a year, from shortly after their initial turnon near mid-1997 until the present. The bulk of the data are from the L modes, although some observations in the M modes provide useful complementary information. Examples of the data in each mode are illustrated, providing an overview of the STIS first-order capabilities. Any changes in the average CCD sensitivities are less than 1%/yr. The formal slope of the fit to the monitoring data and  $1\sigma$  uncertainties are G230LB:  $+0.56\%/\text{yr} \pm 0.29$ , G430L:  $-0.07\%/\text{yr} \pm 0.27$ , G750L:  $+0.19\%/\text{yr} \pm 0.43$ . A small but significant dependence of the G140L sensitivity on temperature, of  $-0.37\%/\text{deg C} \pm 0.06$ , has been found. After the observations are corrected for that effect, the G140L sensitivity changes are also less than 1%/yr ( $0.77 \pm 0.33$ ). The G230L sensitivity is observed to INCREASE at a rate of  $+1.6\%/\text{yr}$  ( $8\sigma$ ) over the entire wavelength range, and by  $2.2\%/\text{yr}$  ( $6\sigma$ ) in the 2200-2400 Å range. Hence, no significant losses of sensitivity due to contamination or any other cause have been observed during this period. After correcting G140L and G230L for temperature and time correlations, respectively, the  $1\sigma$  photometric repeatabilities in broad bands range from 0.3% for G230L to 0.7% for G750L.*

---

## 1. Observations

Programs to monitor the sensitivity of the STIS detectors in spectroscopic modes with external flux standards were begun shortly after they were turned on during SMOV and are continuing through Cycle 7. The primary programs for this purpose during SMOV were Nos. 7063 and 7064 for the CCD and MAMA detectors, respectively, while in Cycle 7 they are Nos. 7672 and 7673. Some data in the same modes from other programs with different primary objectives are also included in this report. All of the datasets analyzed here are listed in Tables 1 and 2, which pertain to the L and M modes, respectively.

The initial SMOV L-mode observations were repeated weekly. In Cycle 7, beginning in August/September 1997, the frequencies are as follows: CCD L modes, every 2 months; CCD M modes, every 4 months; MAMA L modes, monthly; and MAMA M modes, every 4 months initially, increased to every 2 months after May 1998. Various standard targets were used during SMOV and in the other Cycle 7 programs, but Nos. 7672 and 7673 use unique high-latitude standards for each mode. An example of the data in each mode from the latter programs is presented in Figures 1-10.

**Table 1. L-Mode Observations**

Root	Mode	Aper	Target	Date	Time	Propid	Exptime[s]
O3YX14HSM	G140L	52X2	GRW+70D5824	21/06/97	11:08:56	7064	240.0
O3YX15QEM	G140L	52X2	GRW+70D5824	29/06/97	06:08:42	7064	240.0
O3YX16KLM	G140L	52X2	GRW+70D5824	05/07/97	06:40:03	7064	240.0
O43J01QAM	G140L	52X2	GD153	09/07/97	08:54:48	7097	60.0
O3ZX08HHM	G140L	52X2	GD153	13/07/97	04:44:14	7096	187.1
O45901010	G140L	52X2	GRW+70D5824	12/08/97	09:18:10	7673	180.0
O45910010	G140L	52X2	GRW+70D5824	16/09/97	21:11:23	7673	180.0
O45911010	G140L	52X2	GRW+70D5824	06/10/97	13:36:39	7673	180.0
O45912010	G140L	52X2	GRW+70D5824	17/11/97	17:23:40	7673	180.0
O4DD06020	G140L	25MAMA	GD71	30/11/97	11:05:37	7657	120.0
O45913010	G140L	52X2	GRW+70D5824	19/12/97	23:54:46	7673	180.0
O45914010	G140L	52X2	GRW+70D5824	09/01/98	15:03:40	7673	216.0
O45915010	G140L	52X2	GRW+70D5824	12/02/98	14:55:32	7673	189.0
O4PG01N1Q	G140L	52X2	GD71	31/03/98	15:58:37	7917	96.0
O4PG01N9Q	G140L	52X2	GD71	31/03/98	16:07:32	7917	108.0
O4PG01NDQ	G140L	52X2	GD71	31/03/98	16:16:39	7917	108.0
O4PG01NHQ	G140L	52X2	GD71	31/03/98	17:06:45	7917	108.0
O4PG01NPQ	G140L	52X2	GD71	31/03/98	17:15:52	7917	108.0
O45917010	G140L	52X2	GRW+70D5824	12/04/98	17:57:12	7673	204.0
O4SP01060	G140L	52X2	GD71	27/04/98	06:15:01	7932	108.0
O4SP01070	G140L	25MAMA	GD71	27/04/98	06:20:07	7932	108.0
O45940010	G140L	52X2	GRW+70D5824	07/05/98	02:51:18	7673	204.0
O45942010	G140L	52X2	GRW+70D5824	04/07/98	18:54:31	7673	204.0

**Table 1.** L-Mode Observations

Root	Mode	Aper	Target	Date	Time	Propid	Exptime[s]
O45943010	G140L	52X2	GRW+70D5824	05/08/98	07:38:58	7673	204.0
O3YX11P2M	G230L	52X2	GRW+70D5824	29/05/97	22:52:54	7064	636.0
O3YX12UTM	G230L	52X2	GRW+70D5824	06/06/97	00:10:39	7064	636.0
O3YX13TQM	G230L	52X2	GRW+70D5824	13/06/97	21:11:18	7064	636.0
O3YX16KPM	G230L	52X2	GRW+70D5824	05/07/97	06:53:00	7064	636.0
O3ZX08HLM	G230L	52X2	GD153	13/07/97	04:56:19	7096	187.1
O45901020	G230L	52X2	GRW+70D5824	12/08/97	10:14:48	7673	184.0
O45910020	G230L	52X2	GRW+70D5824	16/09/97	21:21:49	7673	184.0
O45911020	G230L	52X2	GRW+70D5824	06/10/97	13:47:05	7673	184.0
O45912020	G230L	52X2	GRW+70D5824	17/11/97	17:34:06	7673	184.0
O4DD07020	G230L	25MAMA	GD71	30/11/97	06:15:45	7657	120.0
O45913020	G230L	52X2	GRW+70D5824	20/12/97	00:05:12	7673	184.0
O45914020	G230L	52X2	GRW+70D5824	09/01/98	15:14:20	7673	216.0
O45915020	G230L	52X2	GRW+70D5824	12/02/98	15:05:45	7673	216.0
O4PG01NTQ	G230L	52X2	GD71	31/03/98	17:27:20	7917	216.0
O45917020	G230L	52X2	GRW+70D5824	12/04/98	18:07:40	7673	204.0
O45940020	G230L	52X2	GRW+70D5824	07/05/98	03:01:46	7673	204.0
O45942020	G230L	52X2	GRW+70D5824	04/07/98	19:04:50	7673	204.0
O45943020	G230L	52X2	GRW+70D5824	05/08/98	07:49:17	7673	204.0
O3TT42010	G230LB	52X2	GD153	21/05/97	10:18:00	7063	600.0
O3TT43010	G230LB	52X2	GD153	28/05/97	06:53:29	7063	600.0
O3TT44010	G230LB	52X2	GD153	04/06/97	11:28:46	7063	600.0
O3TT45010	G230LB	52X2	GD153	10/06/97	22:22:09	7063	600.0
O3TT46010	G230LB	52X2	GD153	18/06/97	04:24:17	7063	600.0
O3TT47010	G230LB	52X2	GD153	25/06/97	04:11:40	7063	600.0
O3TT48010	G230LB	52X2	GD153	01/07/97	12:03:44	7063	600.0
O45A01010	G230LB	52X2	AGK+81D266	03/08/97	00:31:02	7672	144.0
O45A03010	G230LB	52X2	AGK+81D266	01/10/97	05:49:13	7672	144.0
O4D101010	G230LB	52X2	G191B2B	18/10/97	18:27:14	7805	150.0

**Table 1.** L-Mode Observations

Root	Mode	Aper	Target	Date	Time	Propid	Exptime[s]
O4D103010	G230LB	52X2	GD153	12/11/97	01:28:59	7805	400.0
O4D102010	G230LB	52X2	G191B2B	22/11/97	19:10:38	7805	150.0
O45A04010	G230LB	52X2	AGK+81D266	01/12/97	01:43:39	7672	144.0
O4DD03020	G230LB	52X2	GD71	04/01/98	12:06:12	7657	144.0
O45A05010	G230LB	52X2	AGK+81D266	04/02/98	07:59:36	7672	144.0
O45A06010	G230LB	52X2	AGK+81D266	01/04/98	11:00:23	7672	144.0
O45A12010	G230LB	52X2	AGK+81D266	31/05/98	16:13:52	7672	172.8
O45A13010	G230LB	52X2	AGK+81D266	31/07/98	21:27:24	7672	172.8
O3TT42020	G430L	52X2	GD153	21/05/97	10:34:18	7063	252.0
O3TT43020	G430L	52X2	GD153	28/05/97	07:09:44	7063	252.0
O3TT44020	G430L	52X2	GD153	04/06/97	11:45:01	7063	252.0
O3TT45020	G430L	52X2	GD153	10/06/97	22:38:24	7063	252.0
O3TT46020	G430L	52X2	GD153	18/06/97	04:40:32	7063	252.0
O3TT47020	G430L	52X2	GD153	25/06/97	04:27:55	7063	252.0
O3TT48020	G430L	52X2	GD153	01/07/97	12:19:59	7063	252.0
O45A01020	G430L	52X2	AGK+81D266	03/08/97	00:39:41	7672	144.0
O45A03020	G430L	52X2	AGK+81D266	01/10/97	05:57:52	7672	144.0
O4D101020	G430L	52X2	G191B2B	18/10/97	18:35:59	7805	150.0
O4D103020	G430L	52X2	GD153	12/11/97	01:41:54	7805	180.0
O4D102020	G430L	52X2	G191B2B	22/11/97	19:19:23	7805	150.0
O45A04020	G430L	52X2	AGK+81D266	01/12/97	01:52:18	7672	144.0
O45A05020	G430L	52X2	AGK+81D266	04/02/98	08:08:15	7672	144.0
O45A06020	G430L	52X2	AGK+81D266	01/04/98	11:09:02	7672	144.0
O45A12020	G430L	52X2	AGK+81D266	31/05/98	16:23:01	7672	172.8
O45A13020	G430L	52X2	AGK+81D266	31/07/98	21:36:33	7672	172.8
O3TT42040	G750L	52X2	GD153	21/05/97	11:31:25	7063	3240.0
O3TT43040	G750L	52X2	GD153	28/05/97	08:04:35	7063	3240.0
O3TT44040	G750L	52X2	GD153	04/06/97	12:41:08	7063	3240.0
O3TT45040	G750L	52X2	GD153	10/06/97	23:33:17	7063	3240.0

**Table 1. L-Mode Observations**

Root	Mode	Aper	Target	Date	Time	Propid	Exptime[s]
O3TT46040	G750L	52X2	GD153	18/06/97	05:46:23	7063	2282.0
O3TT47040	G750L	52X2	GD153	25/06/97	05:31:49	7063	2282.0
O3TT48040	G750L	52X2	GD153	01/07/97	13:11:51	7063	2282.0
O45A01030	G750L	52X2	AGK+81D266	03/08/97	00:48:20	7672	360.0
O45A03030	G750L	52X2	AGK+81D266	01/10/97	06:06:31	7672	360.0
O4D101030	G750L	52X2	G191B2B	18/10/97	18:44:44	7805	1020.0
O4D103030	G750L	52X2	GD153	12/11/97	01:51:09	7805	740.0
O4D102030	G750L	52X2	G191B2B	22/11/97	19:28:08	7805	1020.0
O45A04030	G750L	52X2	AGK+81D266	01/12/97	02:00:57	7672	360.0
O45A05030	G750L	52X2	AGK+81D266	04/02/98	08:16:54	7672	360.0
O49X07010	G750L	52X2	G191B2B	11/02/98	06:04:24	7674	1980.0
O49X09010	G750L	52X2	GD71	14/02/98	13:10:14	7674	1980.0
O49X08010	G750L	52X2	G191B2B	26/02/98	02:21:52	7674	1980.0
O49X10010	G750L	52X2	GD71	17/03/98	12:59:21	7674	1980.0
O45A06030	G750L	52X2	AGK+81D266	01/04/98	11:17:41	7672	360.0
O45A12030	G750L	52X2	AGK+81D266	31/05/98	16:32:10	7672	432.0
O45A13030	G750L	52X2	AGK+81D266	31/07/98	21:45:42	7672	432.0

**Table 2. M-Mode Observations**

MAMA Program: 7673, CCD Program: 7672, Target: AGK+81D266, Aperture: 52X2

Root	Mode	Cenwave	Gain	Date	Time	Exptime[s]
O45902010	G140M	1567	-	19/09/97	18:13:12	360.0
O45920010	G140M	1567	-	09/01/98	09:48:28	360.0
O45921010	G140M	1567	-	17/05/98	18:35:17	334.0
O45922010	G140M	1567	-	05/07/98	17:12:07	354.0
O45921020	G140M	1173	-	17/05/98	18:48:20	354.0
O45922020	G140M	1173	-	05/07/98	17:25:21	354.0
O45902020	G230M	2818	-	19/09/97	18:27:32	576.0
O45920020	G230M	2818	-	09/01/98	10:02:27	576.0

**Table 2. M-Mode Observations**

MAMA Program: 7673, CCD Program: 7672, Target: AGK+81D266, Aperture: 52X2

Root	Mode	Cenwave	Gain	Date	Time	Exptime[s]
O45921030	G230M	2818	-	17/05/98	19:02:08	570.0
O45922030	G230M	2818	-	05/07/98	17:39:00	570.0
O45A02010	G230MB	1995	1	01/09/97	11:56:05	240.0
O45A07010	G230MB	1995	1	01/01/98	08:37:29	240.0
O45A08010	G230MB	1995	1	18/04/98	00:49:06	240.0
O45A09010	G230MB	1995	1	24/08/98	15:39:43	240.0
O45A02020	G230MB	2416	1	01/09/97	12:06:20	180.0
O45A07020	G230MB	2416	1	01/01/98	08:47:44	180.0
O45A08020	G230MB	2416	1	18/04/98	00:59:21	180.0
O45A09020	G230MB	2416	1	24/08/98	15:49:58	180.0
O45A02030	G430M	3165	1	01/09/97	12:16:05	120.0
O45A07030	G430M	3165	1	01/01/98	08:57:29	120.0
O45A08050	G430M	3165	1	18/04/98	01:20:29	120.0
O45A09050	G430M	3165	1	24/08/98	16:11:06	120.0
O45A08030	G430M	4194	4	18/04/98	01:09:06	120.0
O45A09030	G430M	4194	4	24/08/98	15:59:43	120.0
O45A02040	G430M	4194	1	01/09/97	12:24:00	120.0
O45A07040	G430M	4194	1	01/01/98	09:05:24	120.0
O45A08040	G430M	4194	1	18/04/98	01:12:34	120.0
O45A09040	G430M	4194	1	24/08/98	16:03:11	120.0
O45A02050	G750M	7283	1	01/09/97	12:32:45	120.0
O45A07050	G750M	7283	1	01/01/98	09:14:09	120.0
O45A08060	G750M	7283	1	18/04/98	01:29:14	120.0
O45A09060	G750M	7283	1	24/08/98	16:19:51	120.0

## 2. Analyses

The data have been analyzed independently and in parallel by NRW using IRAF/STS-DAS and by RCB using IDL. The results are in good agreement and have served as useful mutual verifications of the procedures employed.

The IRAF reductions have been based on unfluxed but otherwise calibrated 1D data (available directly from the pipeline since early 1998) and have made use of the following procedures in xstis, in order: thtable, trebin, tchcol, tmerge, tcalc, and tstat. Thtable extracts the relevant row from the STIS data cube into a simple table. Trebin ensures uniform wavelength scales and sampling. Tchcol is used to set the wavelength and net column headings to unique, consecutive values prior to the use of tmerge to include new data into a cumulative master table. Tcalc then divides the new net column by the initial reference one, and tstat provides the mean value and standard deviation of the quotient column.

The results are given in Tables 3 and 4 for the CCD and MAMA, respectively, where the wavelength ranges and bin sizes (which can be inferred from the range and number of points N) are shown for each mode. It should be noted that for the MAMA L modes, only the central wavelength ranges are considered. The reason is that small wavelength shifts and/or scale changes, combined with the rapidly decreasing count rates, caused the steep extremes of the distributions to diverge in the quotients. Initially, small wavelength shifts of about 1 Å or less were applied to the G140L data based on registration of the weak C II 1335 Å interstellar line; however, these shifts did not alleviate the problem and may not have been significant due to the noise in the very weak spectral feature, so they were abandoned after January 1998. Some problems with the pipeline wavelength calibrations were discovered and corrected at about that time. Essentially the entire wavelength ranges are used for the MAMA M and all CCD modes, except that the G750L range beyond 7000 Å subject to strong fringing has been omitted.

**Table 3.** CCD Sensitivity Monitor 1997-1998 (IRAF)  
Program: 7672, Target: AGK+81D266

Ratio	Mean	$\sigma_{mean}$
G230LB (2000-3000 Å, N=501)		
1 Oct/3 Aug	1.006	0.001
1 Dec/3 Aug	1.005	0.001
4 Feb/3 Aug	1.003	0.001

**Table 3. CCD Sensitivity Monitor 1997-1998 (IRAF)**  
**Program: 7672, Target: AGK+81D266**

<b>Ratio</b>	<b>Mean</b>	<b><math>\sigma_{mean}</math></b>
1 Apr/3 Aug	1.008	0.001
31 May/3 Aug	1.007	0.001
31 July/3 Aug	1.006	0.001
G230MB (1920-2070 Å, N=301)		
1 Jan/1 Sept	0.999	0.002
18 Apr/1 Sept	1.013	0.003
24 Aug/1 Sept	1.000	0.0045
G230MB (2340-2490 Å, N=301)		
1 Jan/1 Sept	1.004	0.002
18 Apr/1 Sept	1.007	0.002
24 Aug/1 Sept	1.003	0.003
G430L (3100-5500 Å, N=601)		
1 Oct/3 Aug	0.991	0.001
1 Dec/3 Aug	0.997	0.0005
4 Feb/3 Aug	1.010	0.001
1 Apr/3 Aug	1.009	0.0005
31 May/3 Aug	1.000	0.001
31 July/3 Aug	1.006	0.001
G430M (3050-3300 Å, N=501)		
1 Jan/1 Sept	0.998	0.001
18 Apr/1 Sept	0.996	0.001
24 Aug/1 Sept	0.990	0.001
G430M (4060-4320 Å, N=521)		
1 Jan/1 Sept	0.993	0.001
18 Apr/1 Sept	0.993	0.001
24 Aug/1 Sept	0.991	0.003
18 Apr Gain1/4	4.050	0.004
24 Aug Gain1/4	4.031	0.004
G750L (5600-7000 Å, N=234)		

**Table 3.** CCD Sensitivity Monitor 1997-1998 (IRAF)  
 Program: 7672, Target: AGK+81D266

Ratio	Mean	$\sigma_{mean}$
1 Oct/3 Aug	0.996	0.0015
1 Dec/3 Aug	0.996	0.001
4 Feb/3 Aug	1.002	0.001
1 Apr/3 Aug	1.002	0.001
31 May/3 Aug	1.005	0.0015
31 July/3 Aug	1.005	0.0015
G750M (7000-7500 Å, N=501)		
1 Jan/1 Sept	0.991	0.0015
18 Apr/1 Sept	0.991	0.002
24 Aug/1 Sept	0.986	0.002

**Table 4.** MAMA Sensitivity Monitor 1997-1998 (IRAF)  
 Programs: 7673&7064, L Target: GRW+70D5824, M Target: AGK+81D266

Ratio	Mean	$\sigma_{mean}$
G140L (1300-1500 Å, N=201)		
5 July/12 Aug	0.999	0.002
16 Sept/12 Aug	0.986	0.001
6 Oct/12 Aug	0.992	0.001
17 Nov/12 Aug	0.986	0.001
19 Dec/12 Aug	0.989	0.001
9 Jan/12 Aug	0.979	0.002
12 Feb/12 Aug	0.995	0.002
12 Apr/12 Aug	0.986	0.0015
7 May/12 Aug	0.982	0.002
4 July/12 Aug	0.997	0.002
5 Aug/12 Aug	0.987	0.002
9 Jan/16 Sept	0.992	0.002
7 May/16 Sept	0.996	0.002

**Table 4.** MAMA Sensitivity Monitor 1997-1998 (IRAF)  
 Programs: 7673&7064, L Target: GRW+70D5824, M Target: AGK+81D266

Ratio	Mean	$\sigma_{mean}$
4 July/16 Sept	1.011	0.002
4 July/7 May	1.015	0.002
G140M (1542-1592 Å, N=501)		
9 Jan/19 Sept	0.996	0.002
17 May/19 Sept	0.9965	0.002
5 July/19 Sept	1.000	0.003
G140M (1150-1190 Å, N=401)		
5 July/17 May	1.005	0.0025
G230L (2200-2600 Å, N=401)		
5 July/12 Aug	1.002	0.001
16 Sept/12 Aug	1.001	0.001
6 Oct/12 Aug	1.003	0.001
17 Nov/12 Aug	1.006	0.001
19 Dec/12 Aug	1.007	0.001
9 Jan/12 Aug	1.009	0.001
12 Feb/12 Aug	1.010	0.001
12 Apr/12 Aug	1.017	0.001
7 May/12 Aug	1.018	0.001
4 July/12 Aug	1.014	0.001
5 Aug/12 Aug	1.016	0.001
9 Jan/16 Sept	1.008	0.001
7 May/16 Sept	1.018	0.001
4 July/16 Sept	1.014	0.001
G230M (2775-2860 Å, N=851)		
9 Jan/19 Sept	1.007	0.002
17 May/19 Sept	1.012	0.002
5 July/19 Sept	1.016	0.005

The IDL reductions begin with the raw data for the L modes only, which are calibrated and further analyzed with code specially prepared for the purpose. These reductions are more sophisticated than the IRAF ones in several additional respects. Except for G230L, which has none, the data are aligned on spectral features (the strong Ly $\alpha$  line in the case of G140L); and the count ratios are derived separately for several wavelength bins within the full range of each mode. The longer wavelengths of G750L have been corrected for fringing by means of contemporaneous flats. Because of the larger scatter in the G140L results, a comparison with the charge-amplifier temperatures at the time of each observation was performed, and a correlation that reduces the scatter was indeed found. Another difference between the IDL and IRAF reductions is that in the former, the sensitivity reference is the average of all observations, while in the latter a fixed initial value is adopted. The IDL approach has the disadvantage that the reference is a function of time, but the advantages that the trends are not biased by a possibly anomalous single reference point and that the reference data reduce noise in the ratios by almost the square root of 2. In any event, the results of the two analyses are in agreement. The IDL results are presented in Figures 11-22, which are discussed in the next section.

### 3. Results

The IRAF CCD results given in Table 3 show no significant trends and are consistent with no changes at all in the sensitivities. An amplifier gain check has been included in the G430M observations. These two observations plus three more gain measurements in SMOV give an average of  $4.034 \pm 0.010$  for the actual gain=4 to gain=1 ratio.

The IRAF MAMA results in Table 4 are more interesting. First of all, the behaviors of G140L and G230L are significantly different. Furthermore, these differences are consistently tracked by (the more limited) respective M-mode data, strongly indicating that they are real and related to the detectors rather than the gratings. (Note that separate groups of ratios at the bottoms of the L-mode sections approximately match the M-mode time intervals.) In particular, the G140L ratios are usually less than unity and show significant scatter. Initially there was concern that a 1-2% drop in sensitivity had occurred between August and September 1997, and that a declining trend might be continuing thereafter through January 1998. However, high values recurred subsequently and the appearance became more that of a scatter about a constant value. As discussed in the IDL results below, most of the anomalous behavior of G140L is removed by a correlation with amplifier temperature. Surprisingly, the G230L results in Table 4 show a consistent rising trend, by 1.5-2% over the year of observation. Again, note that G230M behaves identically. The behavior of G230L is confirmed by the IDL analysis below. No obvious physical explanation of this effect comes immediately to mind, except perhaps for a migration of cathode material into the microchannel-plate pores.

The IDL results for the three CCD and two MAMA L modes are summarized in Figure 11 and are presented in more detail in the subsequent figures. As in the IRAF analysis, the CCD modes show no significant trends or variations, even as a function of wavelength in the IDL analysis. The MAMA modes show some marginally significant differences as a function of wavelength, while G230L displays the same global increase in sensitivity as the IRAF results.

Figures 12-17 present the IDL results for the three CCD L modes in greater detail. There is a pair of figures for each mode in turn; the first shows results for individual wavelength bins as a function of time, and the second an average over the full wavelength range. As specified on the plots by the slope of the fits along with the  $1\sigma$  uncertainty in the slope, there are no statistically significant trends or variations, to an upper limit of 1%/yr.

Figures 18-20 present the IDL results for G140L. Figure 18 shows the correlation between sensitivity and amplifier temperature (OM1CAT), by which the other G140L IDL presentations have been corrected. The linear fit corresponds to  $-0.37\%/degree\ C \pm 0.06$ . The correlations with several other available temperatures produced no significant reduction in the residuals. Figure 19 shows the temperature-corrected G140L sensitivity trends as a function of time for several wavelength bins separately. Possible declines in sensitivity of 0.9-2.1%/yr in five bins near 1175 and 1475-1625 Å are seen and are significant at the  $3-5\sigma$  levels. These wavelengths correspond to the steep edges of the count-rate distribution, where the rate is dropping rapidly (see Figure 7). Any slight wavelength misalignment has a large effect on the quotient, and the signal-to-noise is relatively lower in these regions. The M-mode data at these same wavelengths will eventually confirm or deny these trends with higher significance, since their count-rate distributions are much flatter; indeed, a G140M 1173 Å setting was added to program No. 7673 in May 1998 for that reason. The few G140M results to date do not indicate any sensitivity losses at these wavelengths (Table 4), but more time is needed for definitive results. Finally, Figure 20 shows the IDL average, temperature-corrected G140L trend over the entire wavelength range, which is significant at only  $\sim 2\sigma$ .

The IDL G230L results are presented in Figures 21-22. Figure 21 shows the sensitivity trends as a function of time in separate wavelength bins, which are all increasing at a statistically significant level of up to  $9\sigma$ . The rate is near 1%/yr at wavelengths longer than 2400 Å, but higher at shorter wavelengths, with an apparent peak of 2.4%/yr at 2250 Å. Figure 22 shows that the wavelength-averaged increase is 1.6%/yr with little scatter and is significant at the  $8\sigma$  level. After this correction for the change in G230L sensitivity with time is made, the formal correlation with temperature is a change of  $+0.02\%/yr \pm 0.15$ , i.e. no correlation of G230L sensitivity with OM2CAT.

## 4. Photometric Precision

While the  $1\sigma$  rms scatter about the fits is written on each of the Figures 13, 15, 17, 20, and 22, only for G230L is there a sensitivity change over time that differs from zero with statistical certainty. The more relevant quantity is the  $1\sigma$  rms scatter of the average signal about unity, after correcting only the G140L and G230L observations for the temperature and time correlations, respectively. These  $1\sigma$  values are the broadband precisions that a GO can expect for high S/N stellar spectrophotometry through the wide 52x2 arcsec slit. Table 5 summarizes these photometric repeatabilities.

**Table 5.** Average Photometric Precision over the Full Wavelength Ranges for the 52x2 Arcsec Slit

Mode	$1\sigma$ (%)
G140L	0.53
G230L	0.29
G230LB	0.42
G430L	0.38
G750L	0.67

## 5. Recommendations

The issues of whether the derived temperature dependence of the G140L sensitivity and secular increase of the G230L sensitivity should be incorporated into the Calstis pipeline reductions must be considered. Corollary issues are whether they should then be adopted for only those modes in which they were measured, or applied to all modes, imaging as well as spectroscopic, with the respective MAMA detectors. As mentioned above, the few M-mode observations to date agree with the L-mode behaviors. Both the FUV and NUV effects are small enough to affect few science programs before next year. On balance, we recommend that these corrections be added to the pipeline for all modes in 1999, if our monitoring programs continue to detect changes that are in agreement with the results presented here.

## 6. Acknowledgement

The Phase II specifications for the SMOV and Cycle 7 monitoring programs were implemented by Anne Gonnella.

## 7. Figures

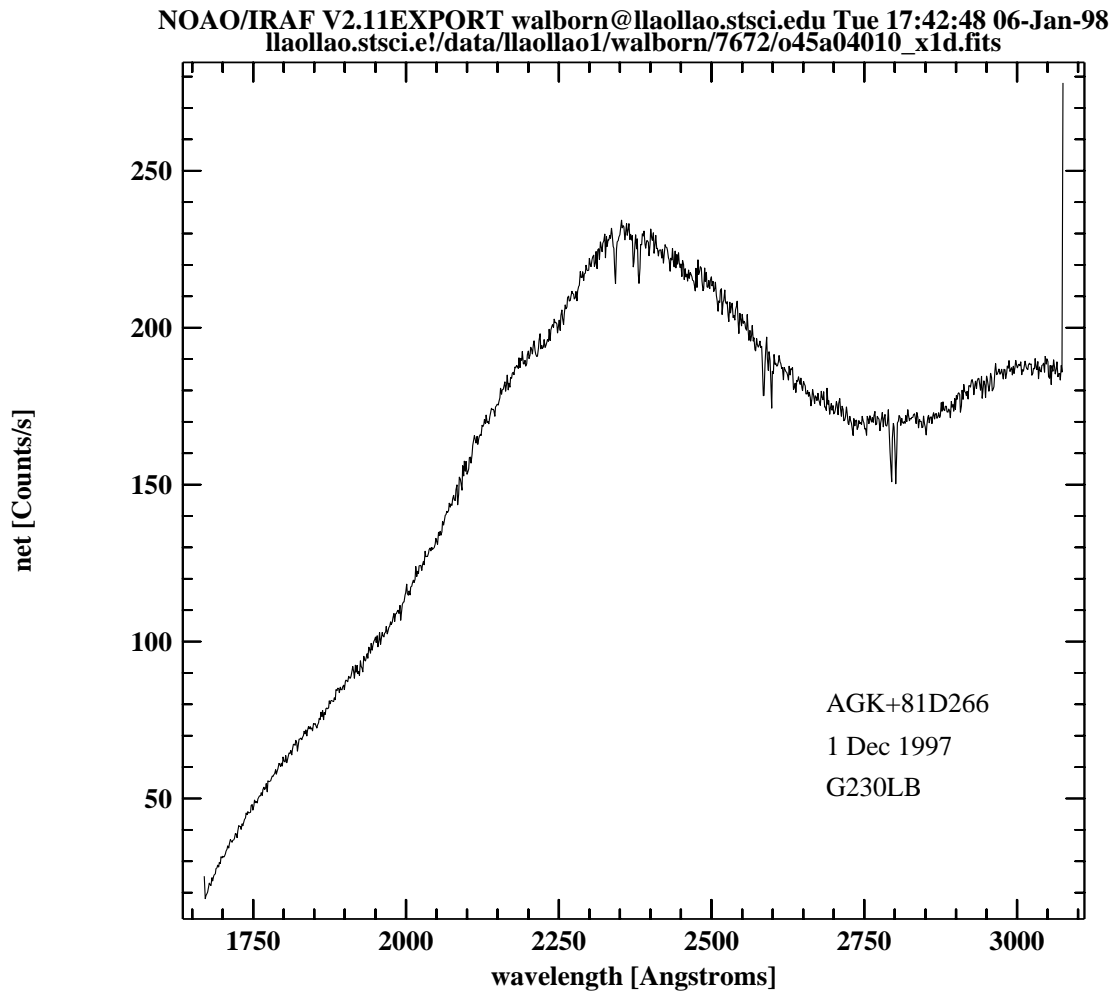


**Figure 1:** G230LB data. Interstellar Fe II 2344, 2374, 2383 Å are prominent, and the interstellar Mg II doublet at 2796, 2803 Å is just resolved. The same features can be compared in the G230MB data of Figure 4 and the G230M data of Figure 10, respectively.

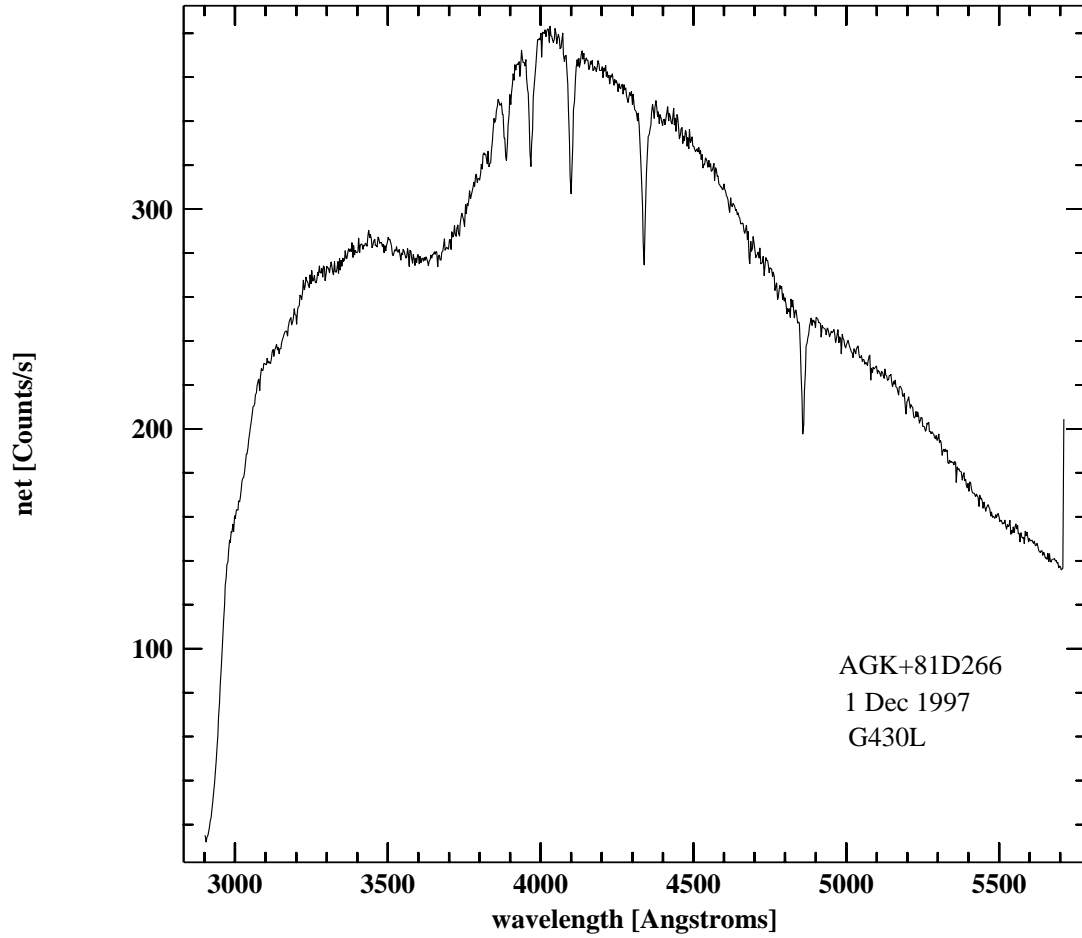


**Figure 2:** G430L data. The stellar Balmer series in this hot subdwarf is prominent from H $\beta$  4861 Å through H $\zeta$  3889 Å.

NOAO/IRAF V2.11EXPORT walborn@llaollao.stsci.edu Tue 17:53:13 06-Jan-98  
llaollao.stsci.e!/data/llaollao1/walborn/7672/o45a04030\_x1d.fits

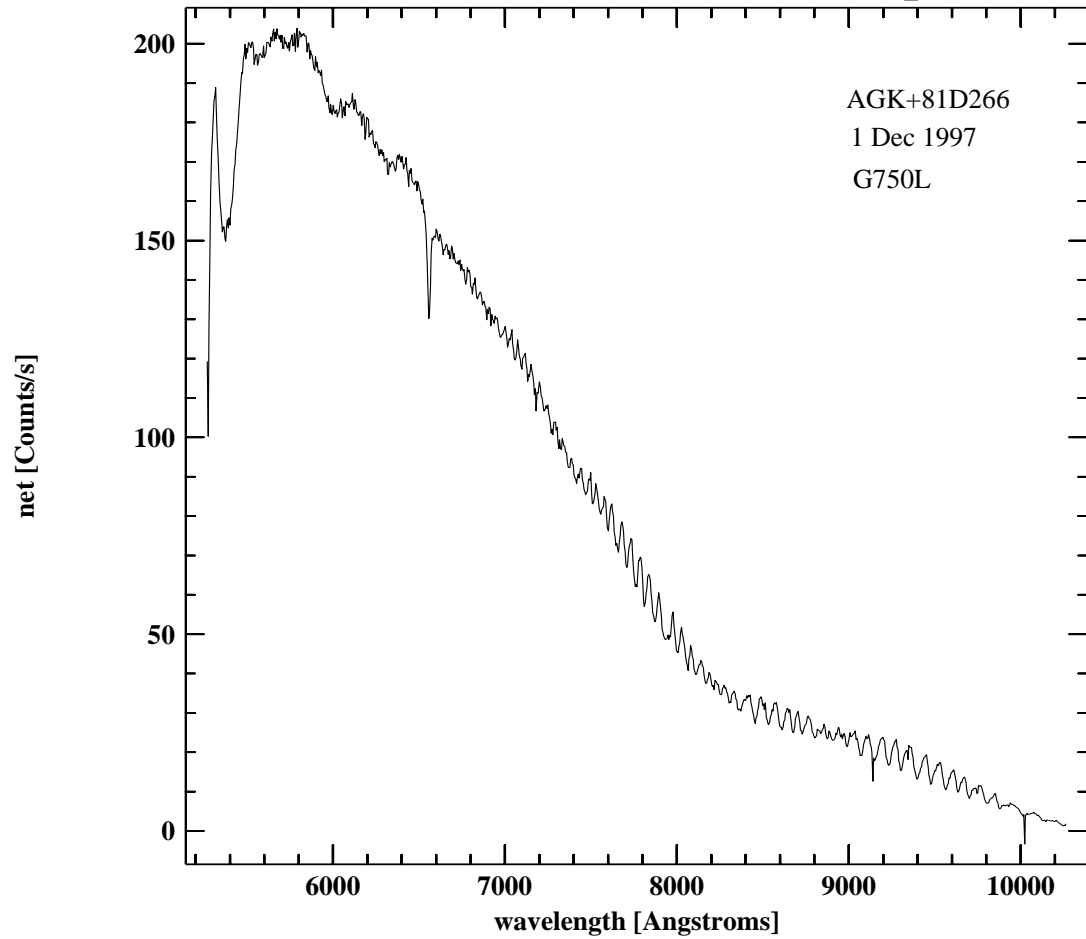


**Figure 3:** G750L data. Stellar H $\alpha$  6563 Å is prominent, as is the (uncorrected) CCD fringing longward of 7000 Å.

NOAO/IRAF V2.11EXPORT walborn@llaollao.stsci.edu Wed 16:13:30 07-Jan-98  
llaollao.stsci.e!/data/llaollao1/walborn/7672/M/o45a07020\_x1d.fits

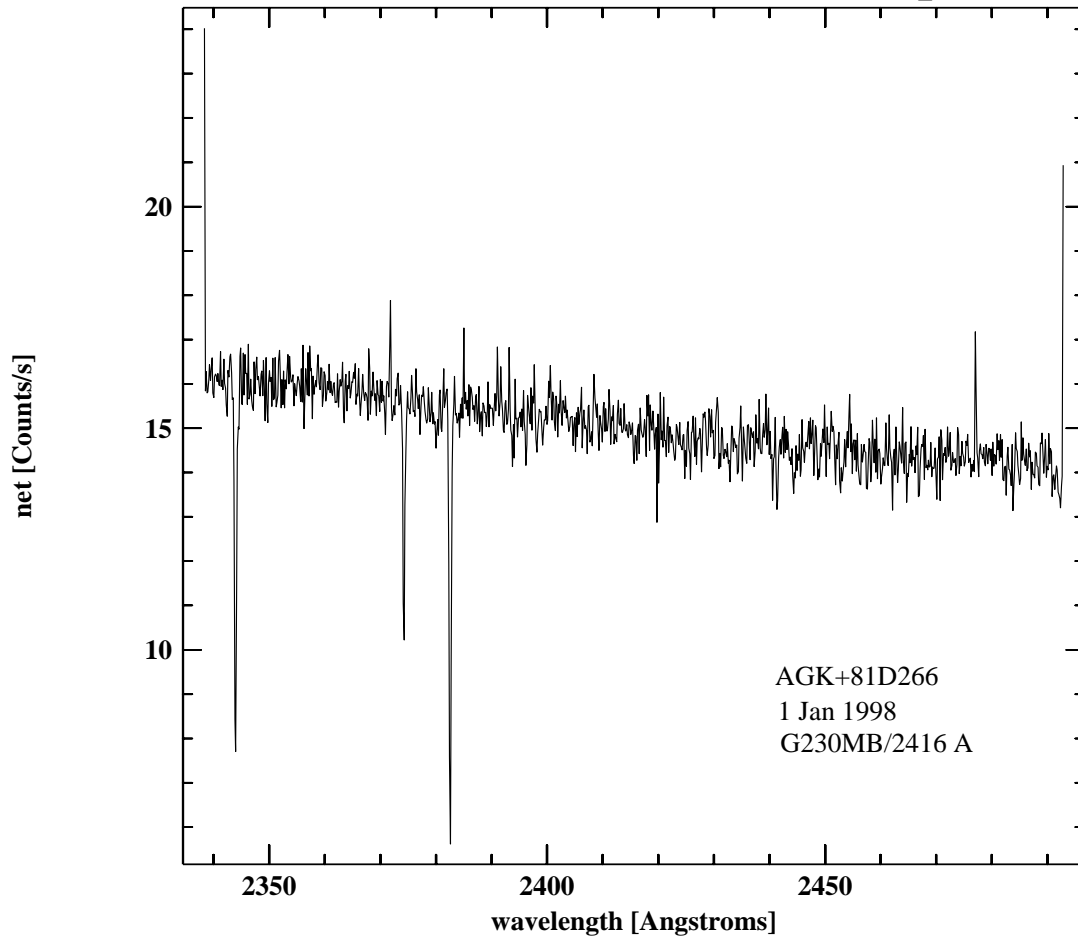


**Figure 4:** G230MB data. Interstellar Fe II 2344, 2374, 2383 Å are prominent; they can be compared with the G230LB data in Figure 1.

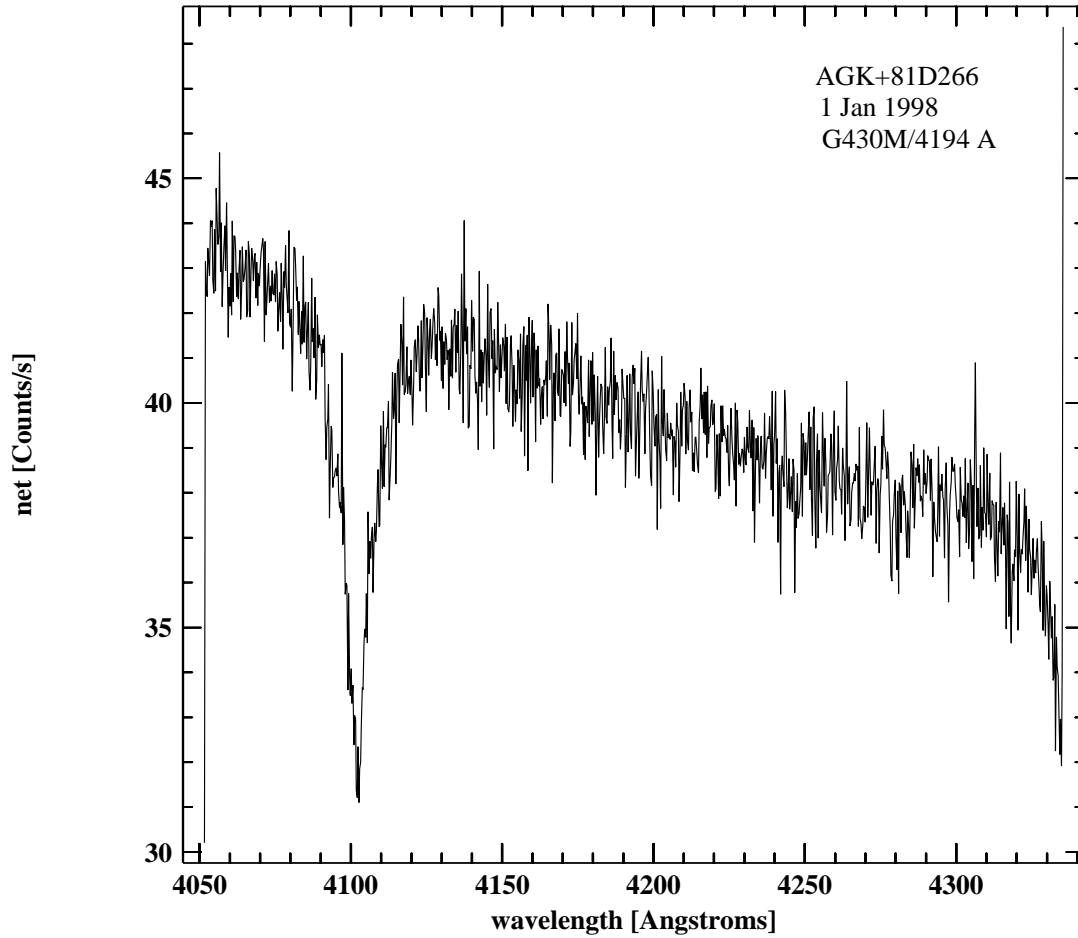


**Figure 5:** G430M data. The strong absorption line is stellar H $\delta$  4102 Å.

NOAO/IRAF V2.11EXPORT walborn@llaollao.stsci.edu Wed 16:48:34 07-Jan-98  
llaollao.stsci.e!/data/llaollao1/walborn/7672/M/o45a07050\_x1d.fits

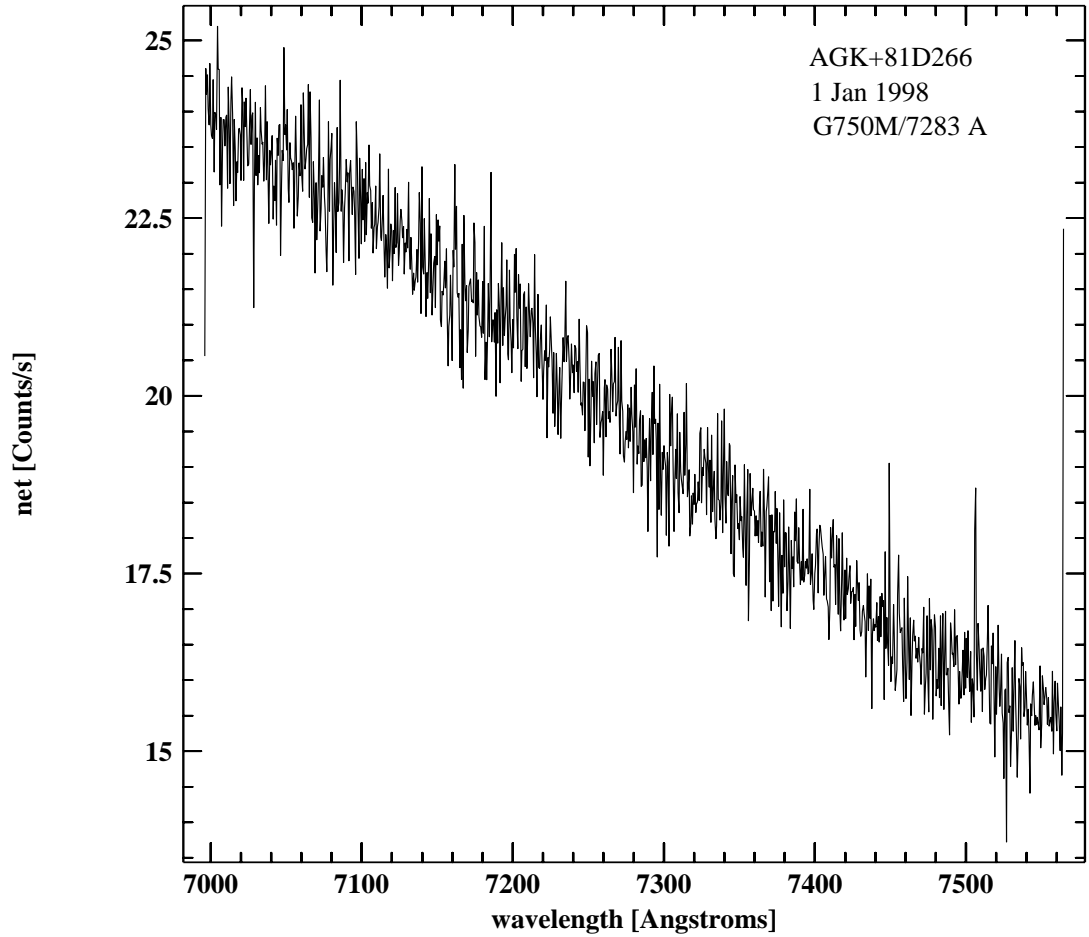
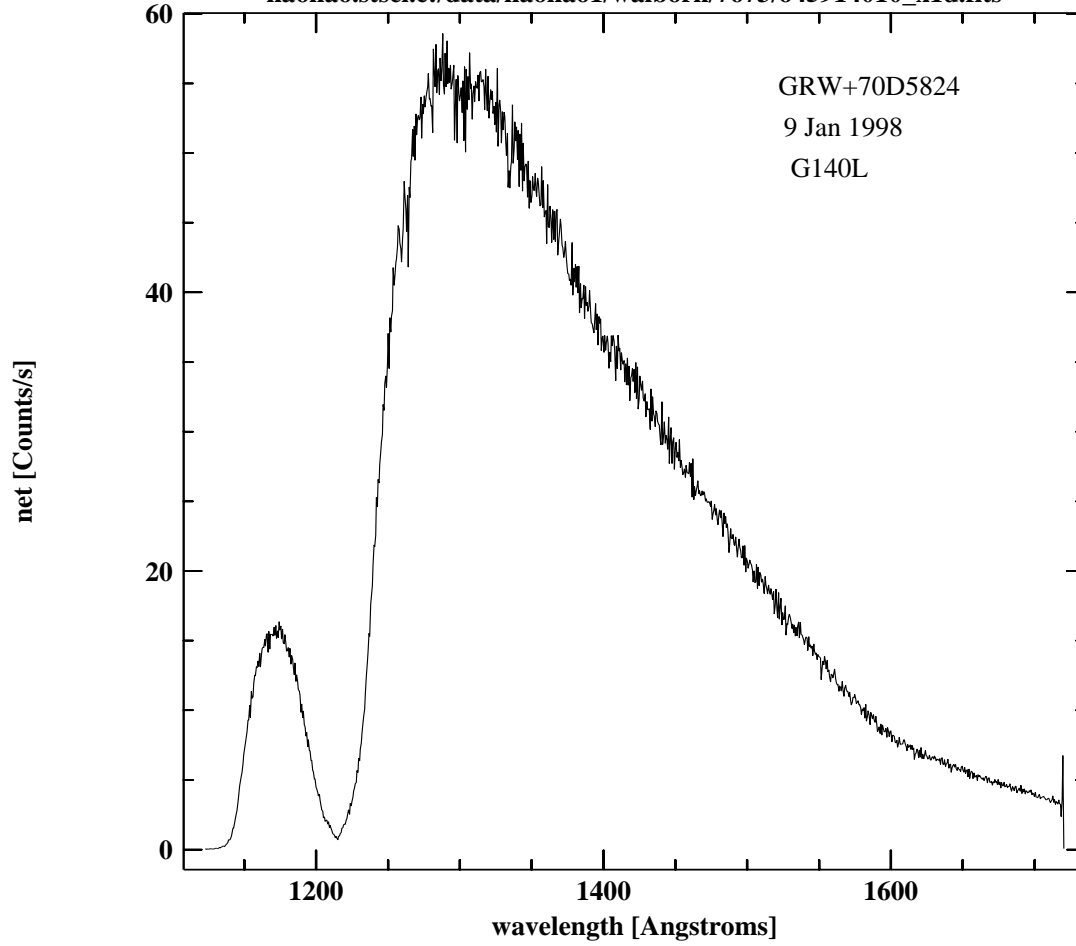


Figure 6: G750M data.

NOAO/IRAF V2.11EXPORT walborn@llaollao.stsci.edu Mon 17:55:24 12-Jan-98  
llaollao.stsci.e!/data/llaollao1/walborn/7673/o45914010\_x1d.fits



**Figure 7:** G140L data. The very strong Ly $\alpha$  1216 Å line in this white dwarf star dominates the count-rate distribution at the shorter wavelengths.

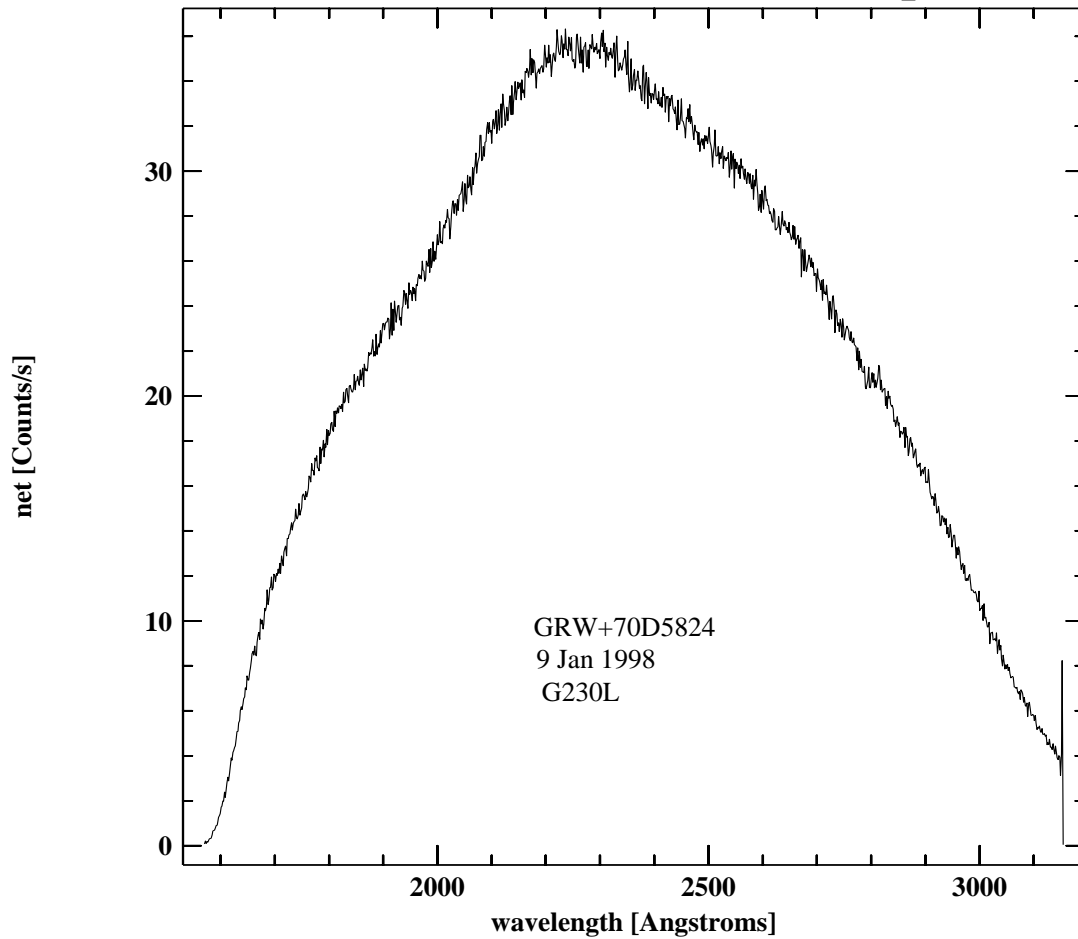
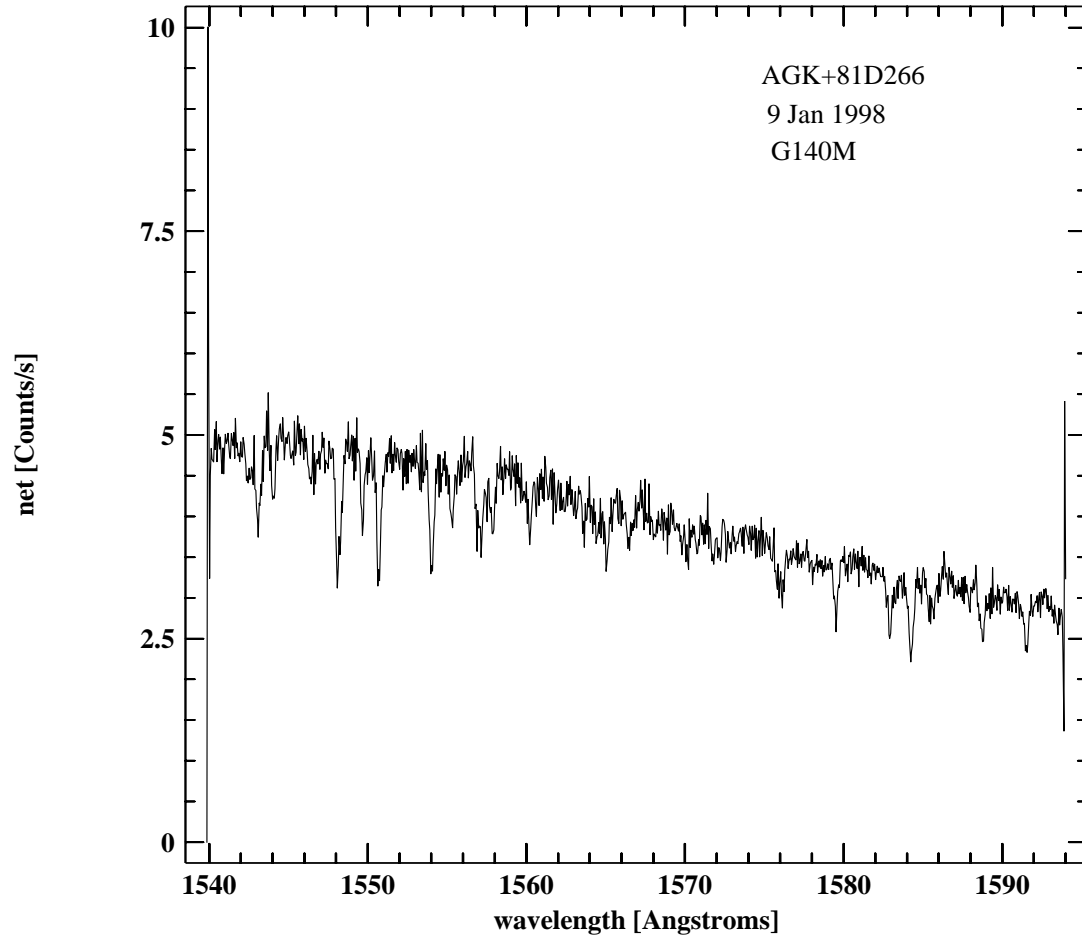


Figure 8: G230L data.

NOAO/IRAF V2.11EXPORT walborn@llaollao.stsci.edu Tue 16:39:20 13-Jan-98  
llaollao.stsci.e!/data/llaollao1/walborn/7673/M/o45920010\_x1d.fits



**Figure 9:** G140M data. The stellar C IV 1548, 1551 Å doublet is prominent in this hot subdwarf.

NOAO/IRAF V2.11EXPORT walborn@llaollao.stsci.edu Thu 15:58:00 22-Jan-98  
llaollao.stsci.e!/data/llaollao1/walborn/7673/M/o45920020\_x1d.fits

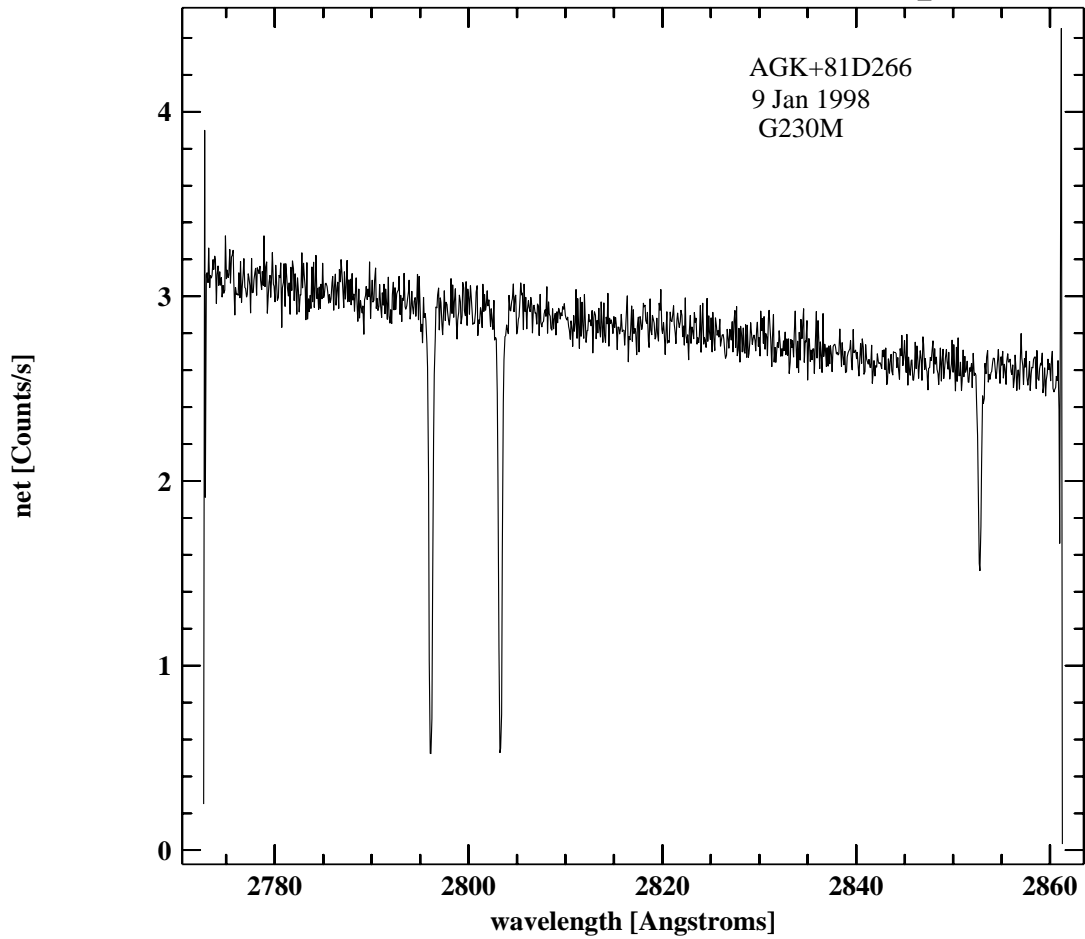
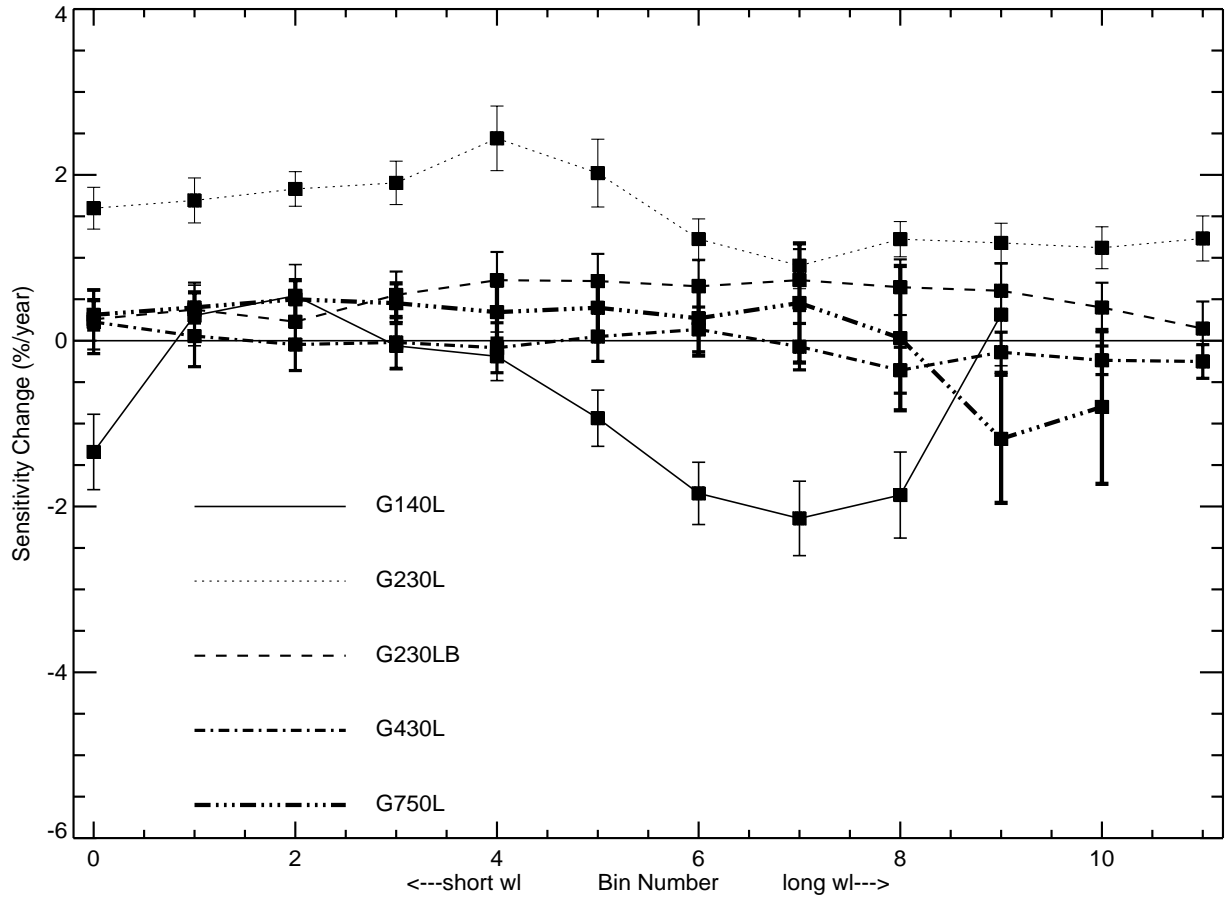


**Figure 10:** G230M data. The strong lines are interstellar Mg II 2796, 2803 Å and Mg I 2853 Å; they can be compared with the G230LB data in Figure 1.



BOHLIN: pltchang 17-Sep-1998 15:33

**Figure 11:** Summary of L-mode sensitivity changes as a function of wavelength bins. The wavelengths of the bins for each mode are specified in subsequent figures. The %/yr changes are from linear fits to the data.

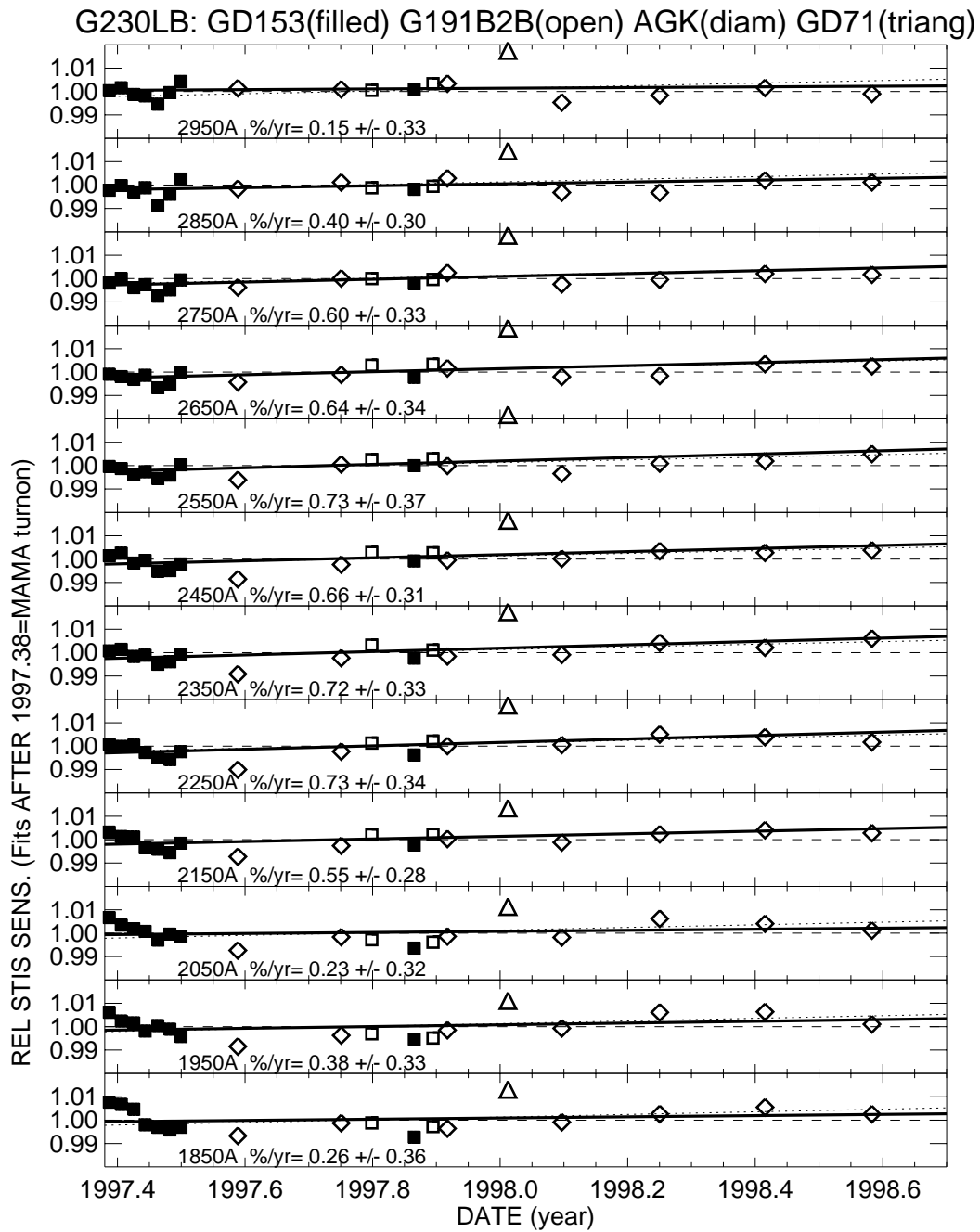
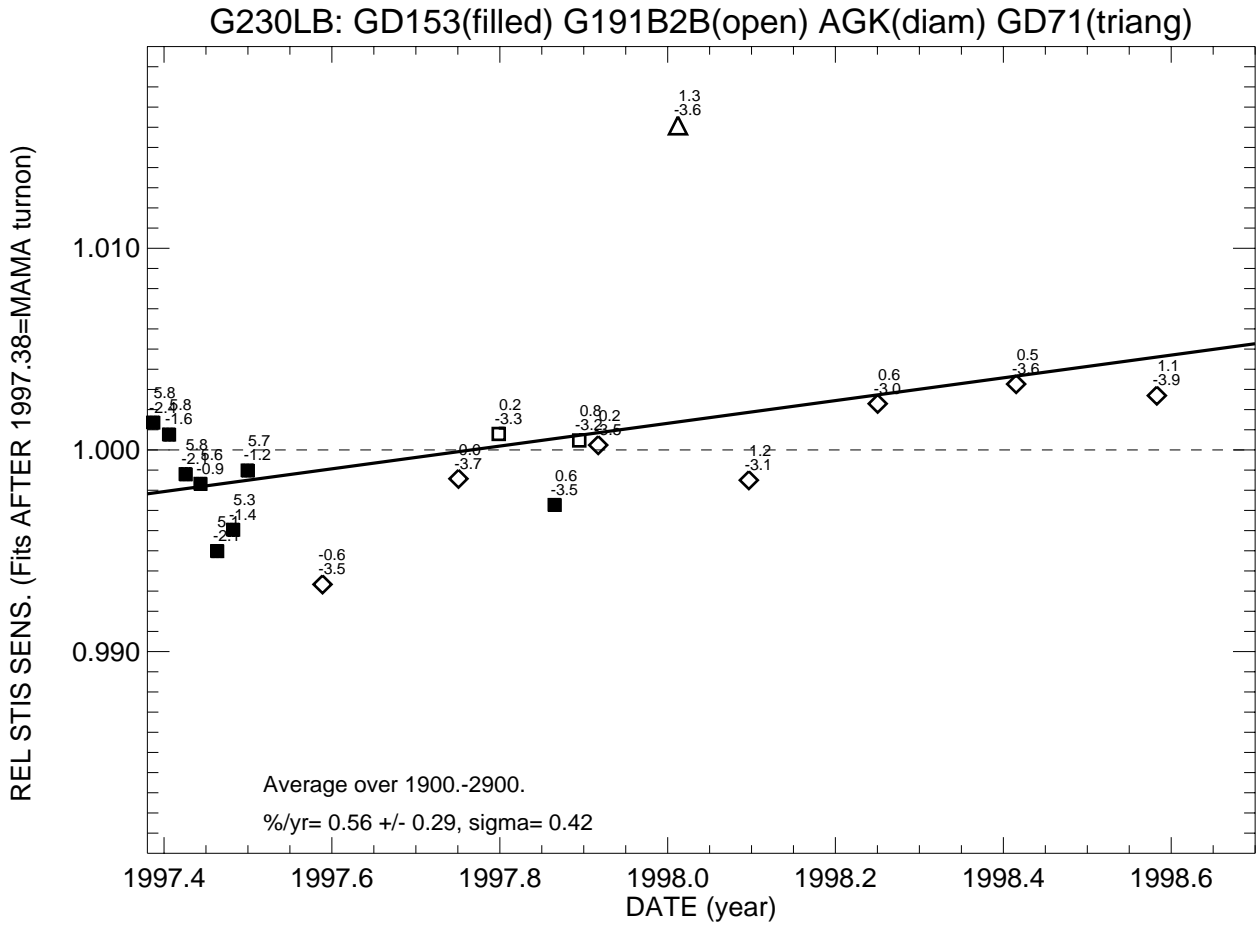
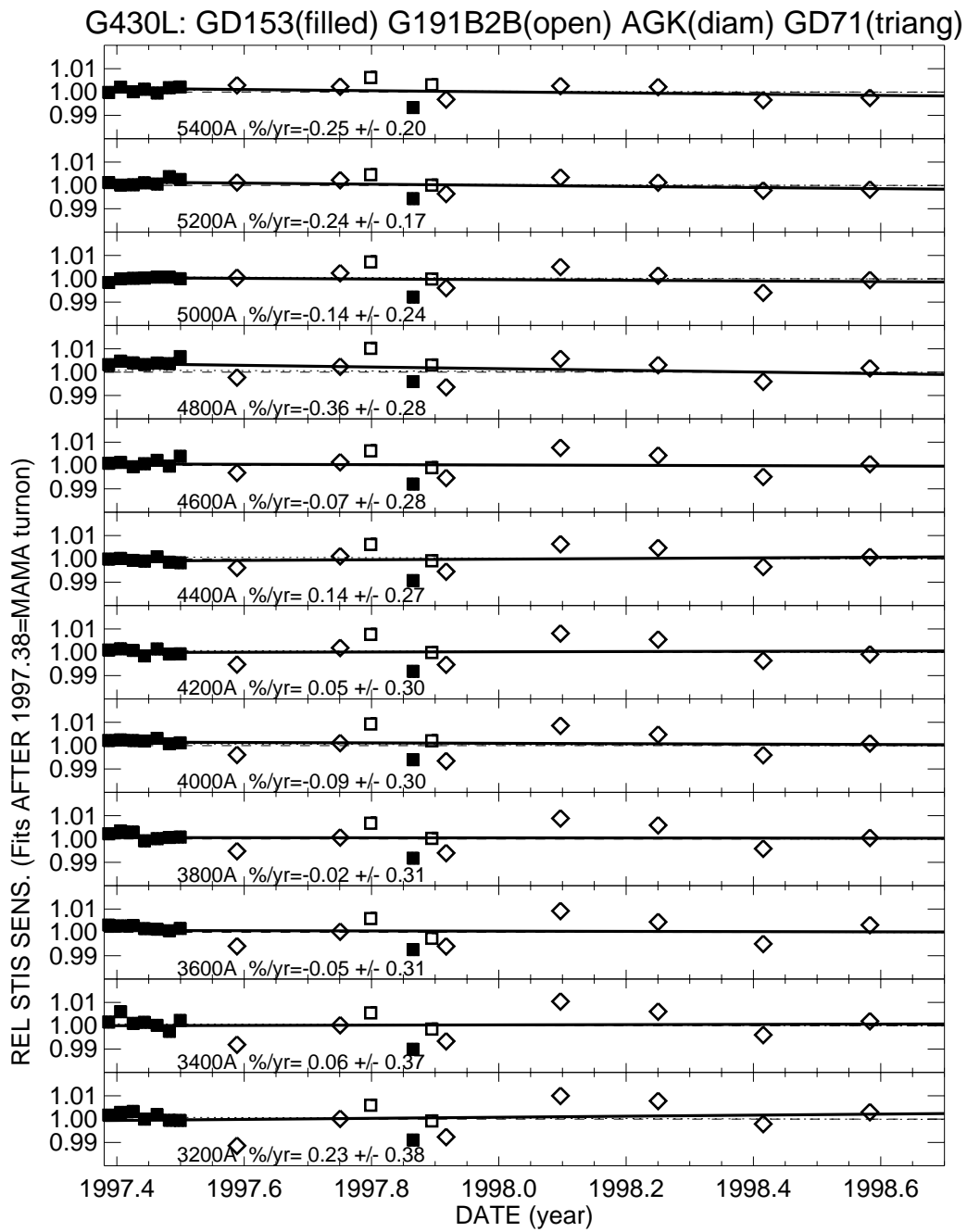


**Figure 12:** G230LB relative sensitivities as a function of time and wavelength bin. The coefficients in %/yr for the linear fits and their  $1\sigma$  uncertainties are written on the plot.



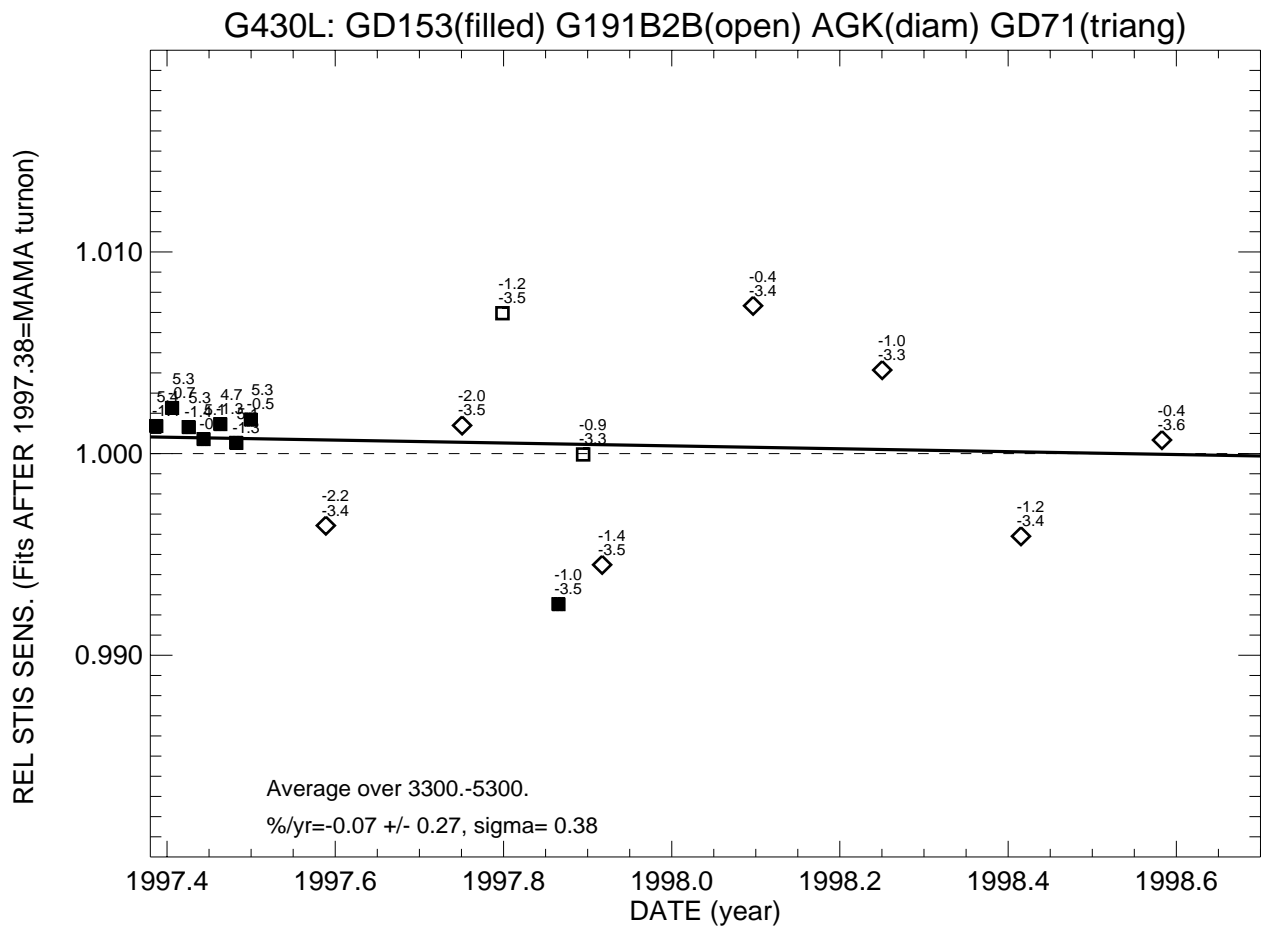
BOHLIN: MAKE-TCHANG 17-Sep-1998 15:29

**Figure 13:** G230LB relative sensitivity as a function of time averaged over wavelength. The pairs of numbers by each point give the pixel offsets of the spectrograms with respect to the image centers, with x above and y below. The coefficient in %/yr for the linear fit, its  $1\sigma$  uncertainty, and the  $1\sigma$  rms scatter about the fit are written on the plot.



BOHLIN: MAKE-TCHANG 17-Sep-1998 15:29

**Figure 14:** G430L relative sensitivities as a function of time and wavelength bin, as in Figure 12.



BOHLIN: MAKE-TCHANG 17-Sep-1998 15:29

**Figure 15:** G430L relative sensitivity as a function of time averaged over wavelength, as in Figure 13.

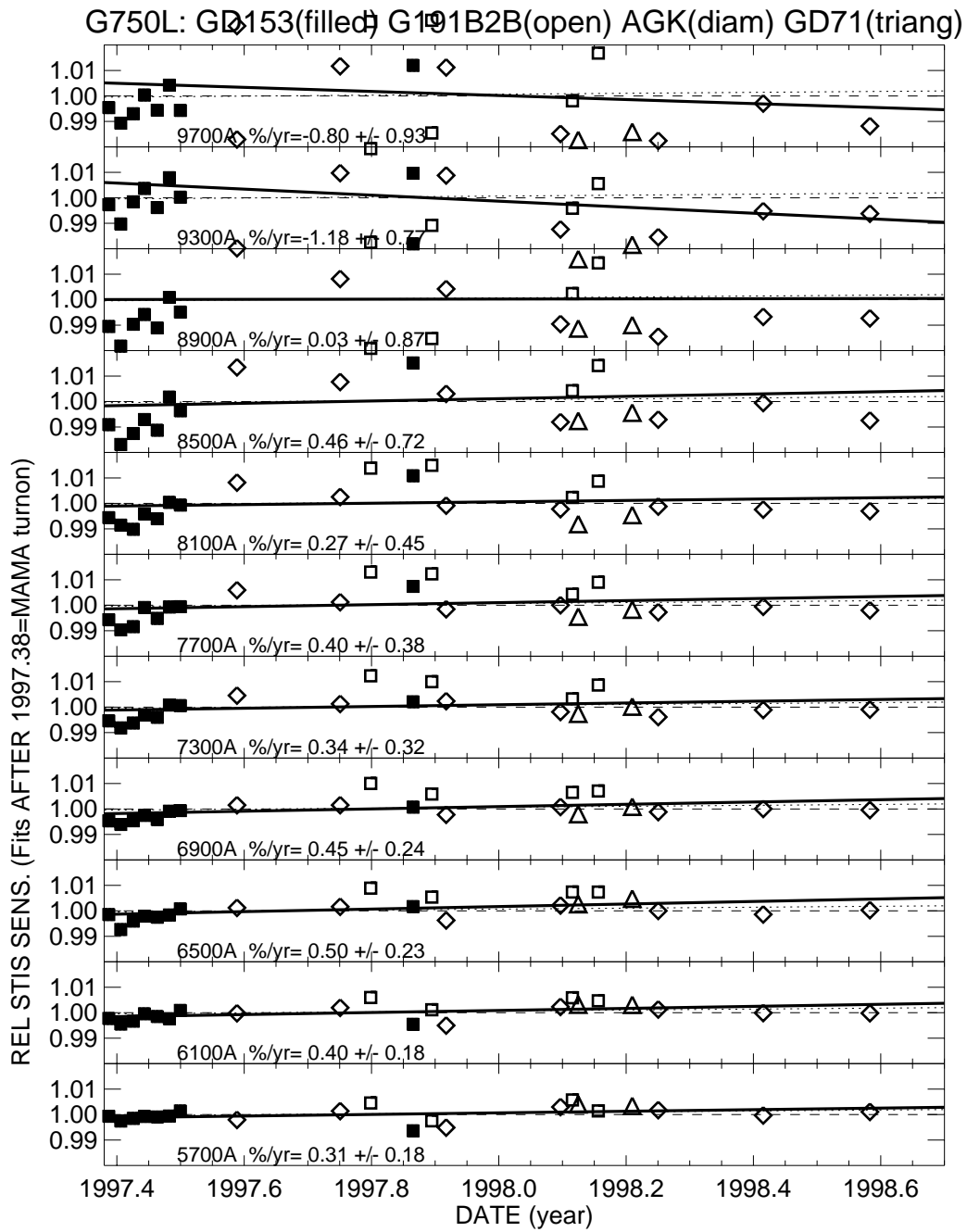
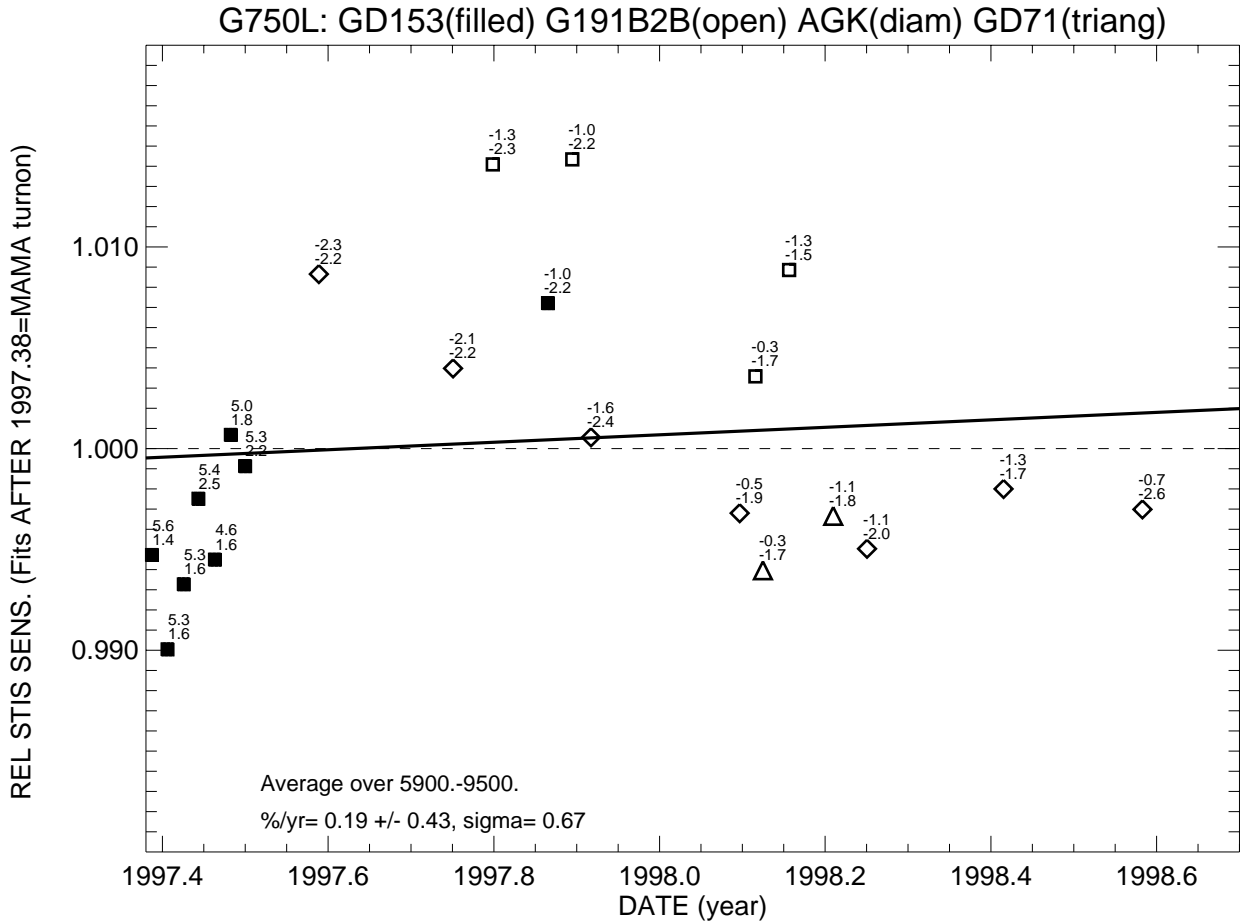
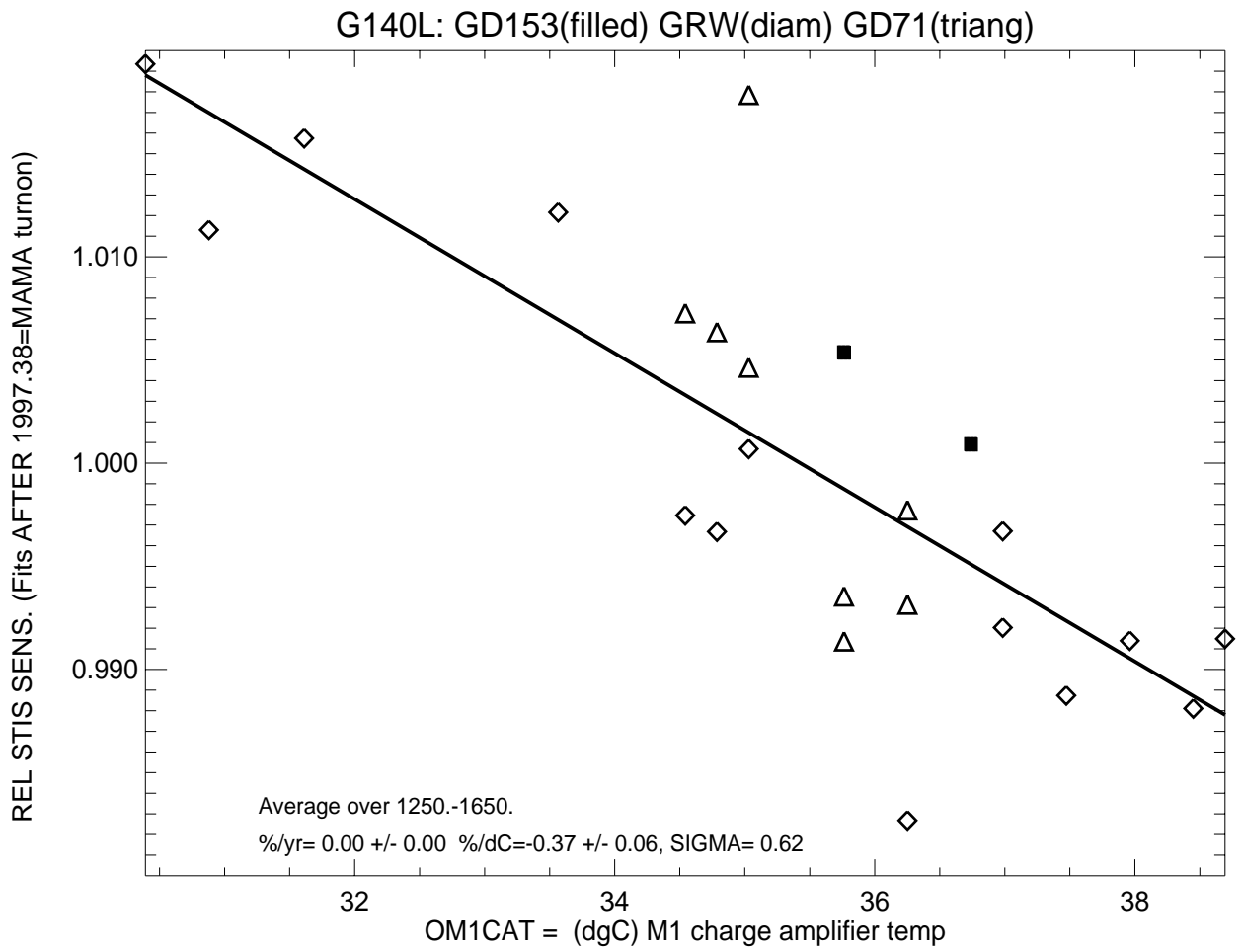


**Figure 16:** G750L relative sensitivities as a function of time and wavelength bin, as in Figure 12.



BOHLIN: MAKE-TCHANG 17-Sep-1998 15:29

**Figure 17:** G750L relative sensitivity as a function of time averaged over wavelength, as in Figure 13.



BOHLIN: Tcorrel 17-Sep-1998 15:36

**Figure 18:** Correlation between G140L relative sensitivity and FUV-MAMA charge amplifier temperature.

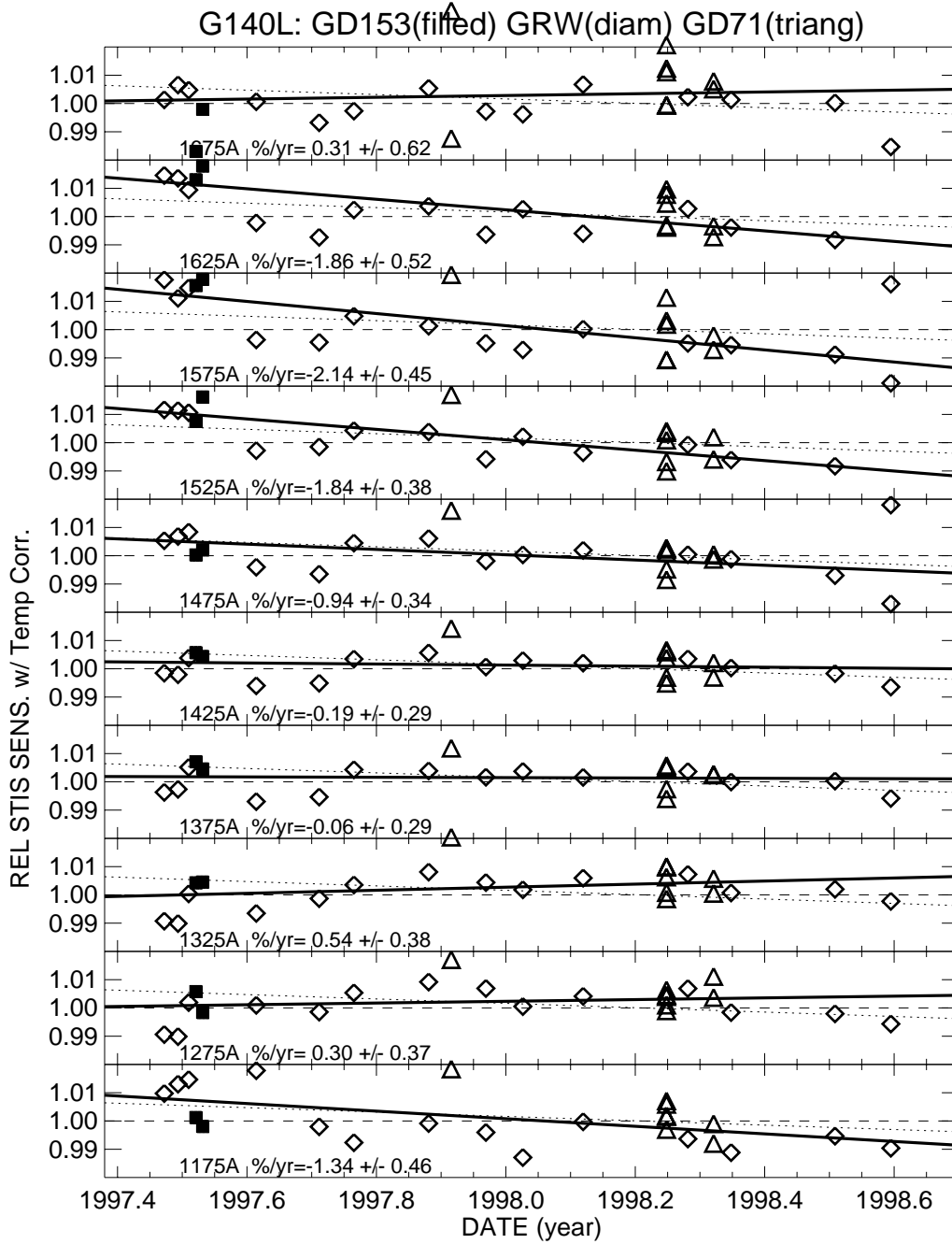
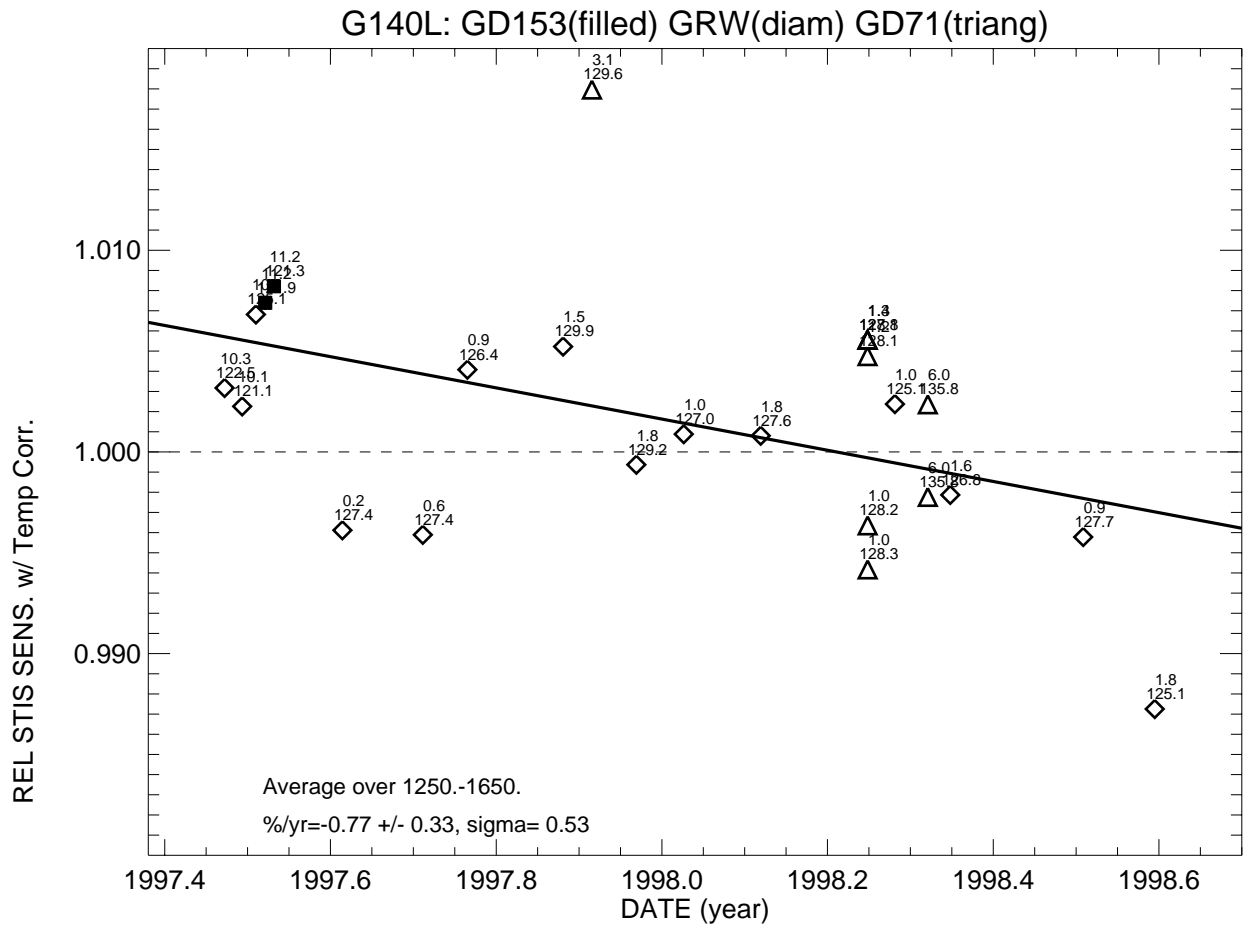


**Figure 19:** G140L relative sensitivities as a function of time and wavelength bin, as in Figure 12.



BOHLIN: MAKE-TCHANG 17-Sep-1998 15:27

**Figure 20:** G140L relative sensitivity as a function of time averaged over wavelength, as in Figure 13. The G140L observations have large y displacements in order to avoid the FUV-MAMA repeller wire.

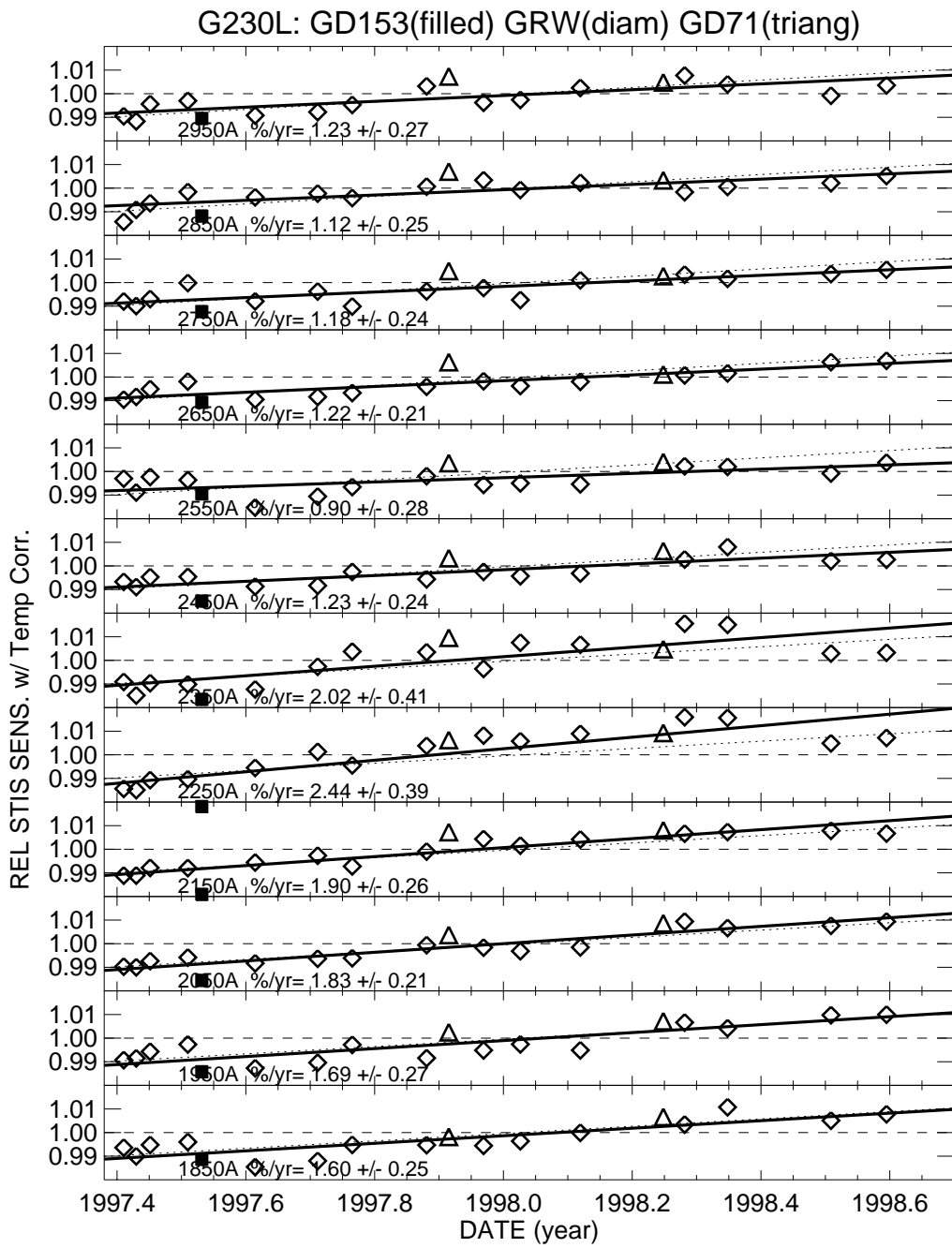
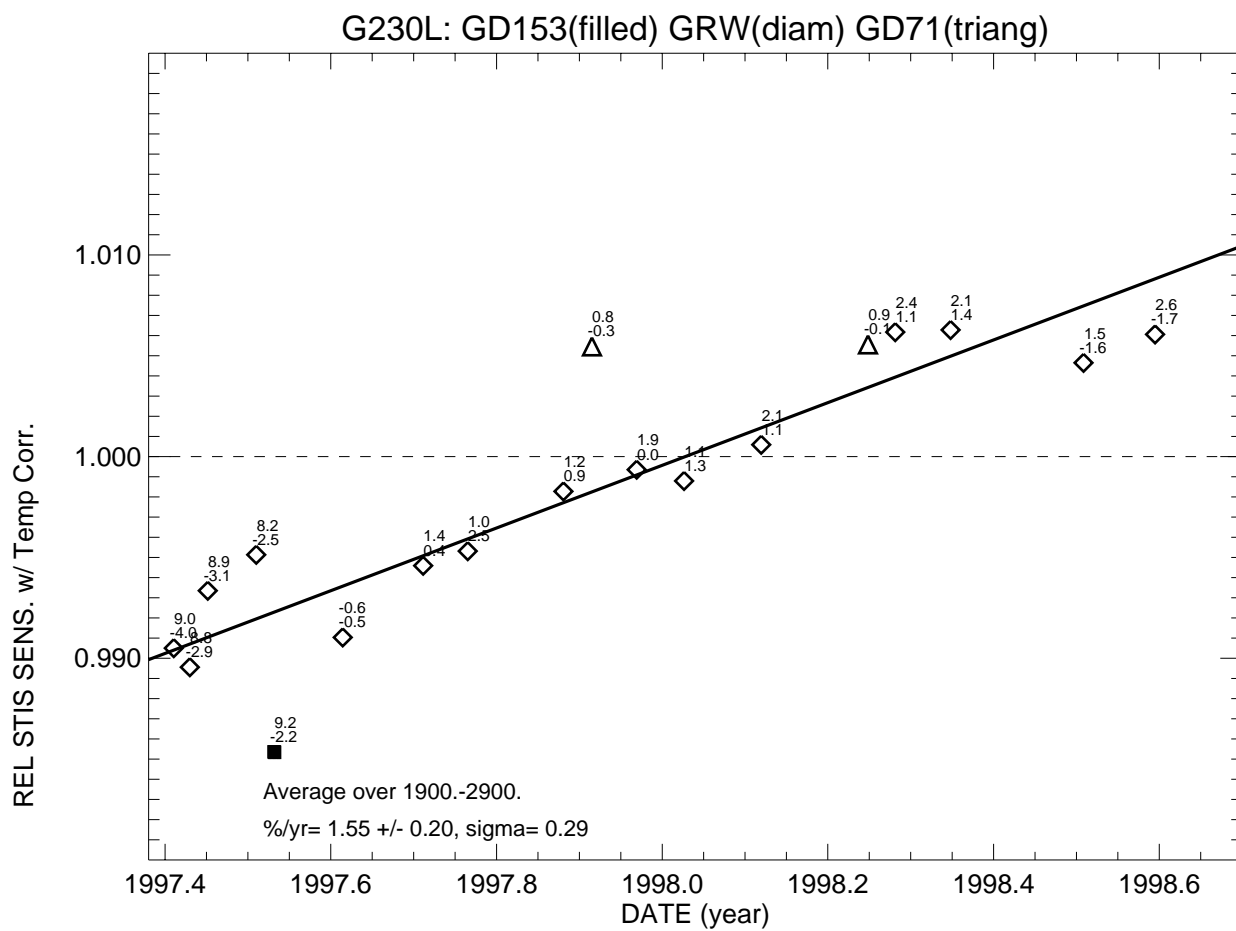


**Figure 21:** G230L relative sensitivities as a function of time and wavelength bin, as in Figure 12.



BOHLIN: MAKE-TCHANG 17-Sep-1998 15:28

**Figure 22:** G230L relative sensitivity as a function of time averaged over wavelength, as in Figure 13.